HHS Public Access

Author manuscript

J Immunol. Author manuscript; available in PMC 2022 March 15.

Published in final edited form as:

J Immunol. 2021 March 15; 206(6): 1297–1314. doi:10.4049/jimmunol.2000965.

TLR3-activated monocyte-derived dendritic cells trigger progression from acute viral infection to chronic disease in the lung

Xinyu Wang[*], **Kangyun Wu**[*], **Shamus P. Keeler**, **Dailing Mao**, **Eugene V. Agapov**, **Yong Zhang**, **Michael J. Holtzman**

Pulmonary and Critical Care Medicine, Department of Medicine, Washington University School of Medicine, St. Louis, MO 63110

Abstract

Acute infection is implicated as a trigger for chronic inflammatory disease but the full basis for this switch is uncertain. Here we examine this issue using a mouse model of chronic lung disease that develops after respiratory infection with a natural pathogen (Sendai virus). We investigate this model using a combination of TLR3-deficient mice and adoptive transfer of immune cells into these mice versus the comparable responses in wild-type mice. We found that acute and transient expression of TLR3 on monocyte-derived dendritic cells (moDCs) was selectively required to induce long-term expression of IL-33 and consequent type 2 immune-driven lung disease. Unexpectedly, moDC participation was not based on canonical TLR3 signaling and relied instead on a trophic effect to expand the alveolar epithelial type 2 (AT2) cell population beyond repair of tissue injury and thereby provide an enriched and persistent cell source of IL-33 required for progression to a disease phenotype that includes lung inflammation, hyperreactivity, excess mucus production, and remodeling. The findings thereby provide a framework wherein viral infection activates TLR3 in moDCs as a front-line immune cell niche upstream of lung epithelial cells to drive the type 2 immune response leading to chronic inflammatory diseases of the lung (such as asthma and chronic obstructive pulmonary disease in humans) and perhaps progressive and long-term post-viral disease in general.

Introduction

To prevent the development of chronic inflammatory disease, it would seem critical to determine the early events that initiate the disease process. It is possible that infection might trigger this process but a clear connection between acute infection and chronic disease as well as a corresponding immune mechanism remain uncertain. A useful paradigm for understanding this issue is represented by one of the most common types of chronic inflammatory disease, i.e., the spectrum of chronic lung disease that includes asthma and

Address correspondence to Michael J. Holtzman., Washington University School of Medicine, Campus Box 8052, 660 South Euclid Avenue, St. Louis, MO 63110. Tel. 314-362-8970; Fax: 314-362-9009; mjholtzman@wustl.edu.

[*]Contributed equally.

Conflict of Interest Disclosures

MJ Holtzman declares that he is a member of the Data Safety Monitoring Board for AstraZeneca and is the founder for NuPeak Therapeutics Inc. The other authors declare no competing financial interests.

chronic obstructive pulmonary disease (COPD) (1–3). Moreover, these types of diseases are subject to initiation, exacerbation, and/or progression due to infection particularly with respiratory viruses (4). A critical challenge then is to determine the nature of the immune response that is responsible for connecting acute respiratory viral infection to chronic inflammatory lung disease.

In that regard, the development of a mouse model of chronic lung disease that develops after virus infection has implicated a central role for the innate immune system in the disease process. In this model, infection with a natural pathogen known as Sendai virus (SeV) leads to expansion and activation of a subset of lung epithelial cells as a source of cytokine IL-33 and in turn immune cell production of IL-13 and consequent airway inflammation, hyperreactivity, mucus production, and structural remodeling (5–11). This innate immune axis is relevant to human disease since the same immune components are implicated in the initiation, exacerbation, and/or progression of chronic and often progressive lung disease in the form of asthma or COPD (6, 7, 12, 13). Moreover, a similar progression from illness to disease after clearance of infectious virus might also occur after severe respiratory viral infections in general, including influenza virus and coronavirus as found in Covid-19 (14, 15).

In the present work, we aimed to better define the initial events that trigger the downstream activation of the IL-33/IL-13-driven type 2 immune response for inflammatory lung disease after respiratory viral infection. We recognized that respiratory viruses (including SeV) rapidly activate several types of pathogen recognition receptors (PRRs), including TLRs (notably TLR3, TLR7, and TLR8), RIG-I-like receptors (RLRs such as RIG-I and MDA-5), and NOD-like receptors (NLRs such as NALP3) (4). This early recognition system is actuated in concert with the recruitment of immune cells such as tissue macrophages that are presumably helpful for repair of cell and tissue injury (9, 16–20). However, any link between these acute illness events and the subsequent development of chronic disease was uncertain. Indeed, it was difficult to understand why this type of disease would develop long after infection virus is cleared and injury is repaired. Initial insight into an upstream immune mechanism was provided from our recent report of the response to SeV infection in *Csf1*-deficient *wt/opT* mice that are missing the population of myeloid-macrophage lineage cells. This deficiency resulted in a marked attenuation in the usual expansion of alveolar epithelial type 2 (AT2) cells (11) that are generally thought to be responsible for at least some aspects of post-viral lung repair (21). However, this population is also the primary source of IL-33 in the mouse lung (11, 22–24), so loss of the myeloid-macrophage lineage cells also blocked the IL-33-driven type 2 immune-response responsible for post-viral disease. Here, we extend this work to show that monocyte-derived dendritic cells (moDCs) provide this trophic signal to a progressive and excessive AT2 cell expansion and further that moDCs require early activation of TLR3 signaling to function as a front-line immune cell niche for expansion of AT2 cells. This finding results in a revision of the conventional view of the epithelial-immune cell interface in the development of inflammatory disease after viral infection proposed in the past (4). We thereby define an early and upstream immune cell event that is required for long-term inflammatory disease and appears relevant to virus-linked lung diseases such as asthma, COPD, and the progressive dysfunction that can develop after any severe respiratory viral infection.

Methods and Materials

Mouse generation and infection

Wild-type C57BL/6J mice (#000664) and *Trif*$^{-/-}$ mice (#005037) were purchased from Jackson Laboratory. The *Tlr3*$^{-/-}$ mice were generated originally by R. Flavell (Yale University, New Haven CT) (25) and were obtained from M. Diamond and M. Colonna (Washington University, St. Louis, MO). All mouse strains were fully backcrossed onto the C57BL/6J genetic background. Mice were infected with SeV (Sendai/52, Fushimi strain) given intranasally (2×10^5 PFU per mouse) or an equivalent amount of ultraviolet light (UV)-inactivated virus or PBS as described previously (26). Viral titers for stock solutions and lung infections were monitored by PCR-based assay as described previously (10). The Animal Studies Committee of the University approved all experimental protocols. Male and female mice (6–10 wk of age) were used for all experiments, however, no significant sex differences were observed in response to viral infection as reported previously (10).

RNA analysis

RNA was purified from homogenized lung tissue using Trizol (Invitrogen) or from isolated cells with the RNeasy mini kit (Qiagen) and was used to generate cDNA with the High-Capacity cDNA Archive kit (Life Technologies). We quantified target mRNA and viral RNA levels using real-time qPCR assay with specific fluorogenic probe-primer combinations and Fast Universal PCR Master Mix systems (Applied Biosystems) with forward and reverse primers and probes as described previously (11) in addition to *Tlr3* for the present work using assay Mm.PT.58.8085919 with forward primer 5'CCTGTATCATATTCTACTCCTTGCT-3', reverse primer 5'-GACGCACCTGTTCTCTATCTG-3', and probe 5'/56-FAM/AACTGCCTG/ZEN/AATCACAATCGCGC/3IABkFQ/-3' from Integrated DNA Technologies. Samples were assayed using the 7300HT or QuantStudio 6 Fast Real-Time PCR System and analyzed using Fast System Software (Applied Biosystems). All real-time PCR data was normalized to the level of *GAPDH* mRNA. Values were expressed as fold-change based on the delta-delta Ct method as described previously (27) with the exception of viral RNA which was quantified by copy number using an *SeV-NP*-expressing plasmid as an internal standard (10).

Histochemistry

Lung tissue was fixed with 10% formalin, embedded in paraffin, cut into 5-μm sections and placed on charged slides. Prior to staining, sections were deparaffinized in Fisherbrand® CitroSolv® (Fisher), hydrated, and heat-treated with antigen unmasking solution (Vector Laboratories, Inc). Sections were stained with PAS and hematoxylin as described previously (10, 14). In addition, immunostaining was performed with the following primary antibodies: anti-MUC5AC (Fisher; clone 45M1), rabbit anti-mouse F4/80 (Cell Signaling, clone D2S9R); chicken anti-GFP (Abcam), goat anti-mouse IL-33 (R&D Systems), and rabbit anti-surfactant protein C (Sftpc; Abcam). For detection of primary Ab binding, sections were incubated in AlexaFluor 488 or 594-conjugated secondary antibodies and counterstained with DAPI-containing mounting media (Vector Labs). Slides were imaged by light microscopy using a Leica DM5000 B microscope and by immunofluorescent microscopy

using an Olympus BX51 microscope, and staining was quantified in whole lung sections using a NanoZoomer S60 slide scanner (Hamamatsu) and ImageJ software as described previously (10, 14).

Flow cytometry

Lung cell suspensions were prepared from lung tissue by mincing followed by digestion in digestion buffer containing collagenase (Liberase Blendzyme III, Roche) and hyaluronidase (Sigma), and DNAse I (grade II, Roche) for 45 min at 37 °C. For epithelial cell isolation, Dispase II (Roche) was added to this buffer. Cells were briefly incubated in ACK Lysing Buffer (Lonza) to lyse RBCs and washed before FcR blockade using anti-mouse CD16/CD32 (Clone 2.4G2; BD Biosciences). The isolated cells were purified using FACS with an iCyt Synergy high-speed flow cytometer (Sony Biotechnology) or FACSAria IIu (BD Biosciences). We used the following anti-mouse antibodies: BV421 anti-CD11b (Clone M1/70; BD Biosciences), PE-Cy7 anti-Ly6G (Clone 1A8, BD Biosciences), FITC anti-CD11c (Clone HL3; BD Biosciences), APC-Cy7 anti-Siglec-F (Clone E50–2440; BD Biosciences), BV421 anti-CD45 (clone 30-F11; BD Biosciences), Alexa Fluor 647 anti-CD64 (clone X54–5/7.1; BD Biosciences), APC-Cy7 anti-EpCAM/CD326 (clone G8.8; BioLegend), PE-Cy7 anti-CD31 (clone MEC 13.3; BD Biosciences), and PerCP-Cy5.5 anti-CD103 (clone M290; BD Biosciences). Specific combinations of mAbs were chosen to identify lung tissue macrophages ($Ly6G^{-}$, $CD11c^{-}$, $Siglec\text{-}F^{-}$, $CD64^{+}$, $CD11b^{+}$), alveolar macrophages ($Ly6G^{-}$, $CD11c^{+}$, $Siglec\text{-}F^{+}$, $CD64^{+}$, $CD11b^{-}$), epithelial cells ($CD45^{-}$, $CD31^{-}$, $EpCAM/CD326^{+}$) and endothelial cells ($CD45^{-}$, $CD31^{+}$, $EpCAM/CD326^{-}$). Dendritic cell subsets were identified as $CD11b^{+}$ DCs ($Ly6G^{-}$, $CD11c^{+}$, $Siglec\text{-}F^{-}$, $CD64^{-}$, $CD11b^{+}$), moDCs ($Ly6G^{-}$, $CD11c^{+}$, $Siglec\text{-}F^{-}$, $CD64^{+}$, $CD11b^{+}$), and $CD103^{+}$DCs ($Ly6G^{-}$, $CD11c^{+}$, $CD64^{+}$, $Siglec\text{-}F^{-}$, $CD11b^{-}$, $CD103^{+}$). For analysis of TLR3 expression, cells were fixed and permeabilized with fixation/permeabilization solution (BD Biosciences) and stained with rat anti-mouse PE TLR3 IgG2a mAb (Clone 11F8, BioLegend). Cells were counted using FACS and fluorescent counting beads (CountBright; Life Technologies). Analysis of flow cytometry data was performed using FlowJo software (Tree Star).

ELISA

Lung tissues were homogenized in T-PER™ Tissue Protein Extraction Reagent (Thermo Fisher Scientific) with protease inhibitor cocktail (cOmplete; Roche) and Halt™ phosphatase inhibitor cocktail (Thermo Fisher Scientific) using a rotor homogenizer (Tissue-Tearor; Biospec Products). Levels of Ccl2, Ccl7, and IL-33 were measured using ELISA kits (R&D Systems and Abcam) and normalized to total protein.

Adoptive cell transfer

For adoptive cell transfer, lung-derived moDCs, tissue macrophages, or bone-marrow-derived dendritic cells (BMDCs) were delivered intranasally (1×10^{6} cells in 30 μl of PBS) to recipient mice as described previously (28, 29). Mice treated identically with intranasal PBS served as controls. All mice were then infected with SeV or PBS control at 1 d after adoptive cell transfer or PBS treatments. The moDCs and tissue macrophages were obtained using FACS-based isolation from lung tissue of mice at 12 d after SeV infection. The BMDCs were generated from cultures derived from bone marrow aspirates maintained in

RPMI containing 10% FBS and recombinant mouse GM-CSF (20 ng/ml; Peprotech) for 8 d at 37 °C changed at 3 and 6 d as described previously (30). The BMDC-enriched nonadherent cells were harvested for adoptive transfer.

Statistical analysis

All data are presented as mean and SEM and are representative of at least three experiments with at least 5 data points per experiment. Unpaired student's t-test with Bonferroni correction as well as mixed-model repeated measures analysis of variance with Tukey correction for multiple comparisons were used to assess statistical significance between means. In all cases, significance threshold was set at $P < 0.05$.

Results

TLR3 influence on acute illness after viral infection

Based on the role of TLR3 as a primary sensor for dsRNA derived from replication of RNA viruses, our initial experiments defined phenotype for *Tlr3*$^{-/-}$ mice during acute illness after SeV infection. We found that the usual decrease in body weight during acute illness was significantly albeit only slightly attenuated in *Tlr3*$^{-/-}$ mice compared to wild-type (WT) control mice (Fig. 1a). In contrast, we observed no significant differences in viral RNA levels during acute illness in *Tlr3*$^{-/-}$ mice compared to WT mice (Fig. 1b), thereby raising the possibility that there might be differences in other aspects of the host immune response. In fact, PAS-hematoxylin staining of lung sections showed a decrease in immune cell accumulation in lung sections from *Tlr3*$^{-/-}$ mice compared to WT mice at 5 d after SeV infection (Fig. 1c) that was significant based on image analysis of hematoxylin^{+} staining (Fig. 1d,e). In addition, we used a flow cytometry scheme for immune cells (Fig. 1f) to show that the increased levels of lung cells and in particular myeloid cells (i.e., tissue macrophages, moDCs, CD11b^{+} DCs, and CD103^{+} DCs) at 5 and/or 12 d after SeV infection were significantly attenuated in *Tlr3*$^{-/-}$ mice compared to WT mice (Fig. 1g). In contrast, levels of alveolar macrophages were increased at baseline and after SeV infection in *Tlr3*$^{-/-}$ compared to WT mice (Fig. 1g), consistent with distinct development and regulation of this cell population (9, 31). Together, the results suggested protection against myeloid cell accumulation and morbidity during acute viral illness in *Tlr3*$^{-/-}$ mice.

TLR3 influence on chronic disease after viral infection

To determine whether TLR3 function might also be linked to the development of chronic post-viral disease, we tested the response of *Tlr3*$^{-/-}$ mice at 49 d after SeV infection when disease phenotype (in particular, immune cell accumulation and mucus production) reach maximal level (6, 8, 10, 11, 32). In contrast to the relatively small effect of Tlr3-deficiency on acute viral illness, we found marked attenuation of hematoxylin staining (reflecting immune and epithelial cell accumulation in this model) and PAS staining (reflecting mucus production) in lung sections from *Tlr3*$^{-/-}$ mice compared to WT mice at 49 d after SeV infection (Fig. 2a,b). Similarly, we observed marked attenuation of the usual increase in mucin 5AC (Muc5ac) immunostaining in lung sections from *Tlr3*$^{-/-}$ mice compared to WT mice at 49 d after SeV infection (Fig. 2c). Each of these effects was significant based on image analysis of hematoxylin^{+}, PAS^{+}, and Muc5ac^{+} staining levels in lung sections from

Tlr3$^{-/-}$ mice compared to WT mice at 49 d after SeV infection (Fig. 2d). In concert with histologic markers of lung disease, we also found that the usual induction of *Il13*, *Muc5ac*, and *Arg1* mRNA in lungs from WT mice, and this response was also markedly decreased in *Tlr3*$^{-/-}$mice at 49 d after SeV infection (Fig. 2e). Similarly, monocyte/macrophage accumulation in lung tissue (marked by immunostaining for F4/80) was markedly attenuated in *Tlr3*$^{-/-}$ mice compared to WT mice at 49 d after SeV infection (Fig. 2f,g). Together, these findings indicate that TLR3 might serve a specific functional role in the type 2 immune response that drives chronic post-viral lung disease.

TLR3 function does not rely on canonical signal transduction

TLR3 (like other TLR) signal transduction is generally thought to be mediated by activation of the downstream adapter protein known as TIR-domain-containing adapter-inducing interferon-β (TRIF) (33, 34). Accordingly, we determined the phenotype of *Trif*$^{-/-}$ mice during acute illness and chronic lung disease after SeV infection.

During acute illness, we found that the usual decrease in body weight was not significantly different in *Trif*$^{-/-}$ mice compared to WT control mice (Fig. 3a). Similarly, we observed no significant differences in viral RNA levels during acute illness in *Trif*$^{-/-}$ mice compared to WT mice (Fig. 3b). Consistent with these findings, PAS-hematoxylin staining of lung sections showed no difference in immune or stromal cell accumulation in lung sections from *Trif*$^{-/-}$ mice compared to WT mice at 5 d after SeV infection (Fig. 3c). This finding was confirmed with quantitative image analysis of hematoxylin^{+} staining (Fig. 3e). In addition, we found that the increased levels of myeloid cells (i.e., tissue macrophages, moDCs, CD11b^{+} DCs, and CD103^{+} DCs) at 5 d and 12 d after SeV infection were often not attenuated (particularly for DCs) in *Trif*$^{-/-}$ mice compared to wild-type (WT) mice (Fig. 3f). Similarly, levels of alveolar macrophages were not increased at baseline and were increased only slightly after SeV infection in *Trif*$^{-/-}$ compared to WT mice (Fig. 3f). Thus, the virus-induced changes in immune cell levels in *Trif*$^{-/-}$ mice were not as pronounced as found in *Tlr3*$^{-/-}$ mice (Fig. 1g). In particular, the results suggested little protection against the accumulation of myeloid cells (especially DCs) and associated morbidity during acute viral illness in *Trif*$^{-/-}$ mice as we had observed in *Tlr3*$^{-/-}$ mice (Fig. 1a–f). In contrast, we found similar induction of monocyte-macrophage chemokine (Ccl2 and Ccl7) production (Fig. 3g) that is dependent on canonical Tlr3 and Trif functions for activating NF-kB-dependent gene expression (35). This data demonstrates that Tlr3-Trif signal transduction is active in this setting but is not sufficient to influence long-term post-viral lung disease.

During chronic disease, we found no significant attenuation of hematoxylin or PAS staining in lung sections from *Trif*$^{-/-}$compared to WT mice at 49 d after SeV infection (Fig. 4a). Similarly, we detected no significant changes in these endpoints based on image analysis of hematoxylin^{+} or PAS^{+} staining levels in lung sections from *Trif*$^{-/-}$ mice compared to WT mice at 49 d after SeV infection (Fig. 4b,c). In concert with histologic markers of lung disease, we also found that the usual induction of *Il13* and *Muc5ac* mRNA was no different in *Trif*$^{-/-}$ mice compared to WT mice at 49 d after SeV infection (Fig. 4d). Together, these findings indicate that TRIF function was not required for the observed changes in either acute illness or chronic disease after SeV infection. These results further suggested TLR3

function in this context depended on an alternative signal transduction pathway to influence acute and chronic effects of SeV infection. Given the initial observation, that some but not all subsets of macrophages might require a TRIF signal (34), we considered whether a specific subset of TLR3-expressing cells might be responsible for the development of post-viral lung disease, recognizing that DCs might be a key target cell type.

moDCs are the most abundant TLR3-high myeloid cells after viral infection

As introduced above, to better understand the how TLR3 might influence acute illness and chronic disease after viral infection, we next defined the cellular site of TLR3 induction and expression. This approach used the same FACS scheme for myeloid macrophage and DC lineage cells as described above (Fig. 1) combined with analysis of lung epithelial cells based on a $CD45^{-}$ $CD31^{-}EpCAM^{+}$ gating scheme as described previously (11). Initial analysis indicated that SeV RNA was localized to each of the myeloid and epithelial cell types with peak viral titers at 5 d that decrease markedly by 12 d after infection (Fig. 5a). Remnant viral RNA at 49 d after infection was detectable primarily in lung epithelial cells, thereby defining the cellular site for persistence found in our analysis of whole lung RNA reported previously (6). In concert with viral RNA levels, we also found that induction of *Tlr3* mRNA expression was also maximal at 5 d after viral SeV infection in each cell subset (Fig. 5b) with the exception of $CD103^{+}$ DCs that are reported to exhibit constitutive expression of *Tlr3* mRNA (36). Similarly, low level *Tlr3* mRNA expression persisted in concert with detection of SeV RNA, particularly in lung epithelial cells (Fig. 5b). Concomitant flow cytometry analysis showed induction of TLR3 protein primarily in moDCs, alveolar macrophages, and epithelial cells at 5 d after SeV infection that returned to near control levels by 12 d after infection (Fig. 5c). Similar to *Tlr3* mRNA levels, TLR3 was expressed on $CD103^{+}$ DCs at similar levels at 0–49 d after SeV infection (Fig 5b,c). These alterations in histograms were confirmed by mean fluorescence index (MFI) for TLR3 signal above background for each cell population (Fig. 5d). Together, the findings indicated that SeV infection induces transient expression of TLR3 at 5 d after infection in moDCs, alveolar macrophages, and lung epithelial cells and leaves constitutive expression on $CD103^{+}$ DCs unchanged, as a starting point for assigning TLR3 function in post-viral lung disease.

In that regard, we also found that the increases in TLR3 expression were accompanied by accumulation of TLR3-expressing myeloid macrophage and DC lineage cells in the lung after viral infection. Thus, we used our flow cytometry scheme (Fig. 1f) to define the full time course for increases in tissue macrophages, moDCs, alveolar macrophages, and $CD11b^{+}$ and $CD103^{+}$ DCs at 0–49 d after SeV infection (Fig. 5e). This analysis indicated that moDCs were the most abundant TLR3-high myeloid cell population early in the course of illness with increases by 5 d after viral infection and the subsequent course with peak levels at 12–21 d after infection (Fig. 5e). These results placed the activation of TLR3-expressing moDCs ahead of the subsequent type 2 immune response that is marked by increases in M2-macrophages, eosinophils, and associated disease traits that are detectable at 21 d and maximal at 49 d after infection (5, 6, 8–11, 13, 14). In contrast, alveolar macrophages exhibit increased TLR3 expression but decreased numbers of cells at 5–12 d after viral infection. Together, these findings like those for TRIF-deficiency suggested a role for $TLR3^{+}$ myeloid cells particularly moDCs in the development of post-viral lung disease.

TLR3 function can be localized to moDCs versus tissue macrophages

Based on the findings that moDCs were the most abundant subset of TLR3-expressing myeloid cells that accumulate in the lung after SeV infection (Fig. 1g and Fig. 5b–d), we examined the possible contribution of this cell population to the development of post-viral lung disease. To define this issue, we isolated moDCs from the lungs of WT and *Tlr3*$^{-/-}$ mice using FACS at 12 d after SeV infection (the peak of moDC levels) and transferred these cells into *Tlr3*$^{-/-}$ mice that were then subjected to SeV infection 1 d later and assessment of lung disease at 49 d after infection (as diagrammed in Fig. 6a). Remarkably, we found that transfer of moDCs from WT but not from *Tlr3*$^{-/-}$ mice fully reconstituted post-viral lung disease at 49 d after SeV infection. In particular, adoptive transfer of WT moDCs restored histopathology (marked by hematoxylin and PAS staining) in lung sections of *Tlr3*$^{-/-}$mice to levels ordinarily found in WT mice at 49 d after SeV infection (Fig. 6b,c). Similarly, we detected the usual increase in Muc5ac immunostaining in lung sections from *Tlr3*$^{-/-}$ mice after WT moDC transfer (Fig. 6d). Each of these effects was significant based on image analysis of hematoxylin^{+}, PAS^{+}, and Muc5ac^{+} staining levels in lung sections from *Tlr3*$^{-/-}$ mice that received WT versus *Tlr3*$^{-/-}$ moDC transfer or control PBS treatment (Fig. 6e). Together, these findings indicate that TLR3 function in moDCs was critical to trigger the progression from acute illness to chronic disease in the lung after SeV infection.

To define the specificity and timing of TLR3-moDC action, we next compared moDC to tissue macrophage function and checked an earlier time point in the disease process. Accordingly, we modified our protocol to include adoptive transfer with both moDCs and tissue macrophages (defined as tissue monocytes plus interstitial macrophages). In addition, we assessed the development of post-viral lung disease at 21 d after SeV infection (when disease is significant but not yet maximal). In this set of experiments (as diagrammed in Fig. 7a), we found that transfer of moDCs but not tissue macrophages from mice reconstituted post-viral lung disease after SeV infection. Thus, adoptive transfer of WT moDCs restored histopathology (marked by hematoxylin and PAS staining) in lung sections of *Tlr3*$^{-/-}$mice to levels found in WT mice at 21 d after SeV infection (Fig. 7b,c). In contrast, the disease was not reconstituted with comparable transfer of WT tissue macrophages (Fig. 7b,c). Each of these effects was significant based on image analysis of hematoxylin^{+} and PAS^{+} staining levels in lung sections from *Tlr3*$^{-/-}$ mice that received WT moDC or tissue macrophage transfer versus control PBS treatment into WT mice (positive control) or *Tlr3*$^{-/-}$ mice (negative control) (Fig. 7d). Together, these findings indicate that TLR3^{+} moDCs but not tissue macrophages are critical to trigger the development of post-viral lung disease in the time window from TLR3 expression and presumably activation (at 5 d after viral infection) to disease onset (at 21 d after infection).

To further define the specificity of moDC participation and any requirement for viral conditioning in post-viral disease, we also studied the capacity of bone-marrow derived dendritic cells (BMDCs) to reconstitute post-viral lung disease. For this approach, we cultured BMDCs from WT or *Tlr3*$^{-/-}$ donor mice before transfer into *Tlr3*$^{-/-}$ recipient mice that then undergo PBS challenge and disease phenotyping (as diagrammed in Fig. 8a). The cells harvested under these culture conditions were significantly enriched in BMDCs (Fig. 8b) as reported previously (30, 37), and thereby allowed for better assignment of TLR3

function to DCs versus other TLR3$^+$ immune-cell populations. Under these cell culture conditions, BMDCs from WT but not *Tlr3*$^{-/-}$ mice exhibit expression of intracellular TLR3 based on flow cytometry analysis (Fig. 8c). To validate our adoptive transfer, we also checked for arrival of adoptive transfer of moDCs in the lung using BMDCs isolated from *CAG-gfp* reporter mice. This approach showed that BMDCs obtained from *CAG-gfp* mice and transferred into *Tlr3*$^{-/-}$ mice can be detected in lung sections generally at parenchymal sites adjacent to alveolar epithelial cells with the morphology of AT2 cells (Fig. 8d). In contrast, transfer with unlabeled cells did not generate a detectable GFP signal as a marker of specific immunostaining (Fig. 8d). Under these conditions, we found that adoptive transfer of WT BMDCs into *Tlr3*$^{-/-}$ mice resulted in barely detectable airway inflammation (marked by immune cell accumulation) and mucus production (marked by PAS staining) that was nonetheless significantly increased when quantified in comparison to control mice (Fig. 8e–g).

Given the minor nature of the observed lung disease after BMDC transfer without viral infection, we next applied the same approach with BMDC transfer into mice followed by SeV infection. In these experiments, we also tracked the time course for detection of transferred BMDCs obtained from CAG-GFP reporter mice. based on serial photomicrographs and quantitation (Fig. 9b,c). We found levels of GFP$^+$ BMDCs in lung sections that are maximal at the time of transfer and are markedly decreased even by 5 d after transfer. This time course resembles the findings that Tlr3 expression and consequent function is also transient after viral infection (e.g., Fig. 3b–d). Indeed, we found that adoptive transfer of these TLR3$^+$ BMDCs results in reconstitution of post-viral lung disease in *Tlr3*$^{-/-}$ mice at 49 d after SeV infection. Thus, transfer of WT BMDCs fully restored histopathology (marked by hematoxylin and PAS staining) in lung sections of *Tlr3*$^{-/-}$mice to levels found in WT mice at 49 d after SeV infection (Fig. 9d). These effects were significant based on image analysis of hematoxylin$^+$ and PAS$^+$ staining levels in lung sections from *Tlr3*$^{-/-}$ mice that received WT BMDCs versus control PBS treatment into WT mice (positive control) or *Tlr3*$^{-/-}$ mice (negative control) (Fig. 9e,f). As noted above, this data remains consistent with transient Tlr3 expression and function after viral infection and the possible requirement for viral infection of moDCs themselves or neighboring cells to fully manifest post-viral disease.

Together, the three sets of adoptive transfer experiments (using moDCs, tissue macrophages, and BMDCs) establish a role for TLR3-activated moDCs in the development of chronic lung disease after SeV infection. In all cases, histopathology showed immune cell infiltration in peribronchial locations with extension to adjacent alveolar tissue in concert with excess mucus production. This bronchoalveolar pattern of disease resembles the histopathology of respiratory viral infection and subsequent consequences of virus-induced lung disease found in our previous studies of mouse models of post-viral disease (10, 11, 14). Further, the deposition of adoptively transferred moDCs near alveolar epithelial cells suggested this site as at least one possible mechanism for moDC function in driving post-viral lung disease.

TLR3$^+$ moDCs drive IL33$^+$ AT2 cell expansion

As introduced above, we next aimed to better define the underlying mechanism for moDC function in post-viral lung disease. Given the accumulation of moDCs and increases in TLR3 expression during the acute illness after viral infection, we first examined type 2 immune events upstream of IL-13 production and consequent mucus production. Indeed, we found significant attenuation of induction of *Il33* mRNA expression in the lungs of *Tlr3*$^{-/-}$ (but not *Trif1*$^{-/-}$) mice compared to WT mice at 49 d after SeV infection (Fig. 10a). The down-regulation of *Il33* mRNA with TLR3-deficiency was accompanied by a similar decrease in induction of IL-33 protein in the lungs of *Tlr3*$^{-/-}$ mice (Fig. 10b). In addition, IL-33 production was restored with moDC transfer from WT (but not *Tlr3*$^{-/-}$) mice into *Tlr3*$^{-/-}$ mice at 49 d after SeV infection (Fig. 10c).

Based on the adjacency of adoptively transferred moDCs to AT2 cells and the role of AT2 cells in IL-33 production during post-viral lung disease (11), we next examined the effect of moDCs on AT2 cells during post-viral disease. In the first set of experiments, we verified that the primary source of *Il33* mRNA after viral infection was the lung epithelial cell population. Thus, FACS separation of lung endothelial, immune, and epithelial cells and subsequent analysis of *Il33* mRNA was able to localize expression to the epithelial cell population (Fig. 10d,e). In addition, we found that the usual expansion of the AT2 cell population at 49 d after infection in WT mice was blocked in *Tlr3*$^{-/-}$ mice based on immunostaining for the AT2 cell marker surfactant protein C (Sftpc) (Fig. 9f) and quantitation of Sftpc$^+$ cells (Fig. 10g). In addition, we found that expansion of the Sftpc$^+$ AT2 cell population at 49 d after SeV infection was restored with moDC transfer from WT (but not *Tlr3*$^{-/-}$) mice into *Tlr3*$^{-/-}$ mice, again based on Sftpc immunostaining and tissue and cell morphology (Fig. 10h) confirmed by quantitation of Sftpc$^+$ cell levels (Fig. 10i). These findings continued to suggest an early effect of TLR3$^+$ moDCs in the disease process that drives Sftpc$^+$ AT2 cell expansion. Indeed, we also found that the attenuation of Sftpc$^+$ AT2 cell expansion in *Tlr3*$^{-/-}$ mice was detected as early as 5 d after SeV infection and then continued to 49 d after infection (Fig. 10j). In addition, we showed that IL-33 expression was primarily localized to Sftpc$^+$ AT2 cells based on immunostaining (Fig. 10k) and that IL-33$^+$Sftpc$^+$ AT2 cells were significantly decreased in *Tlr3*$^{-/-}$ compared to WT mice (Fig. 10k,l). Quantitation showed that the number of IL-33$^+$Sftpc$^+$ AT2 cells were decreased as a percentage of total lung cells without a change in the ratio of IL-33$^+$ to Sftpc$^+$ AT2 cells (Fig. 10l). Thus, TLR3-deficiency resulted in attenuation of AT2 cell expansion without a change in the level of IL-33 expression within AT2 cells. Together, the findings indicated that the early arrival of TLR3$^+$ moDCs is essential for the subsequent and progressive expansion of IL-33-expressing AT2 cells as a mechanism to drive the downstream type 2 immune response responsible for the development of long-term lung disease after SeV infection.

Discussion

This study provides evidence that the development of chronic inflammatory lung disease after respiratory viral infection depends on seminal input from TLR3$^+$ moDCs. This conclusion is supported by findings that: (1) respiratory infection (here using the SeV-mouse

model) causes inducible expression of TLR3 in moDCs in concert with transient viral replication; (2) mice deficient in *Tlr3* but not *Trif* gene expression exhibit decreased acute illness (base on weight loss and inflammation) and marked attenuation of long-term disease that develops and progresses after infectious virus is cleared; (3) adoptive transfer of wild-type moDCs or BMDCs (but not tissue macrophages) into *Tlr3* gene-deficient mice restores the type 2 immune response and consequent disease after viral infection; (4) moDC transfer also restores the excessive expansion of the AT2 cell population that is responsible for IL-33 production and consequent post-viral lung disease. Taken together, the findings provide for a pathway from viral infection to activation of $TLR3^+$ moDCs to drive downstream expansion of $IL\text{-}33^+$ AT2 cells and consequent IL-13 production for a type 2 immune response leading to inflammatory lung disease (as depicted in Fig. 11). Here we discuss how these findings provide unexpected insights for a revised paradigm for post-viral lung disease and the implications for a similar process in humans with lung disease.

The first unconventional aspect of our findings is the role of TLR3 in promoting a progressive, long-term inflammatory disease process. Thus, pathogen recognition receptors such as the TLRs are generally reported to provide a rapidly coordinated response that provides for initial host defense against infection and/or injury. Consistent with this idea, in the present model, TLR3 function contributed to acute illness manifested by weight loss and inflammation. These findings are similar to reports of short-term inflammation in a mouse model of human rhinovirus infection (38), worsened survival after IAV infection (39), and excessive airway inflammation and mucus production in RSV infection (40). Presumably, this response contributes to the call for immune cell influx as a means to halt viral spread, e.g., by recruitment of phagocytic macrophages that control inflammatory debris and antigen-seeking dendritic cells that will arm the adaptive immune response. However, we show here that TLR3 also triggers a long-term inflammatory response that leads to chronic disease even after infectious virus is cleared. The biological rationale for the prolonged type 2 immune response is uncertain but is likely linked at least in part to primordial defense against pathogens via mucociliary clearance (4). In any case, the TLR3 phenotype seems distinct from other PRRs such as melanoma differentiation-associated protein 5 (MDA5) that dampens the inflammatory response to SeV (41). Similarly, TLR3 but not MDA5 disrupts the epithelial barrier in response to dsRNA (42). Further, TLR3 deficiency had no effect on viral RNA levels, likely reflecting a redundant role in the IFN response that is key to control of SeV replication and consequent severity of infection (10, 43). Indeed, stromal cell RIG-I and immune cell TLR7 and TLR8 are each reported to manage the control of SeV replication independent of TLR3 (44). Nonetheless, TLR3 deficiency in humans is marked by herpes simplex virus type 1 (HSV-1) infection as a sign of specificity and complexity for TLR3 function based on tissue and virus type (45). A preliminary report suggests that TLR3 (and TLR4 and TRIF) signals are also protective in a mouse model of SARS-CoV-2 infection based perhaps on controlling viral replication (46), but any understanding of mechanism or translation to humans still needs to be defined.

In that regard, the second unexpected result of the present work is related to the nature of the TLR3 signal transduction pathway for post-viral lung disease. In particular, TLR3 signaling is generally thought to proceed via the TRIF adapter protein as introduced above in the Results section. Instead, TRIF-deficient mice showed no significant change in the acute

illness or the development of chronic lung disease after SeV infection. Non-TRIF-dependent signaling for TLR3 function has been reported previously. Examples include a TRIF-independent branch of TLR3 signaling to c-Src kinase (47). However, this signal actually down-regulates cell motility, adhesion, and proliferation, and therefore appears inconsistent with the present phenotype. Moreover, this pathway was not yet studied in immune cells or in vivo. TLR3 has also been linked to ligand induction for EGFR signaling (48), but in this case the mouse model was performed in a genetic background (Balb/cJ) that does not develop chronic disease after SeV infection (32, 49) and was also not used to address mechanism in vivo. In that regard, others reported that TRIF-deficiency attenuates the response to dsRNA-induced exacerbation of antigen (ovalbumin) challenge (50), but no comparison to TLR3-deficiency was reported to define a difference for allergic versus viral inflammation. Further study of TLR3 signal transduction will also need to account for the complexity of intracellular localization for TLR3 and the N-TLR3–C-TLR3 complex that might be required for signaling (51, 52) as well as TLR3 traffic inside endosomal vesicles (53) and stimulation of inflammatory vesicle traffic (54).

The third result of significance is the identification of moDC participation in long-term post-viral lung disease. As mentioned in the Introduction, our previous work indicated that SeV infection can activate lung macrophages during acute illness via an anti-apoptotic chemokine (CCR5) signal that is key to initial host defense (16). In addition, we found that lung macrophages contribute to IL-13 production and consequent type 2 inflammation based on at least two mechanisms: (1) soluble TREM-2-dependent auto-amplification (9); and (2) synergy with group 2 innate lymphoid cells (ILC2s) (11). The effect on ILC2s coincided with an action of myeloid-macrophage lineage cells on AT2 cell expansion for IL-33 production that in turn is required for ILC2 activation (11). However, the precise nature of the myeloid-macrophage cell type that acted on AT2 cells was not yet defined. Here we demonstrate that moDCs are at least in part responsible for driving increases in AT2 cell and consequent IL-33 levels linked to long-term post-viral lung disease. Others have also described a role for monocyte-derived $CD11b^+$ DCs in an allergen-challenge mouse model of short-term allergic lung disease (55). We also found a similar effect of $Fc\varepsilon RI\alpha^+$ DCs on activation of T cells (in this case $CD4^+$ Th2 cells) after SeV infection that also provides a link to allergic disease (29, 56). However, we also established that $CD4^+$ (and $CD8^+$) conventional T cells are not required for long-term post-viral disease in the present SeV-mouse model (6). Thus, the connection of moDC activation to long-term disease sparks a set of new questions for pathogenesis and the consequent paradigm for chronic inflammatory lung disease.

In that regard, the fourth consequence of our findings is the relatively upstream and presumably early site of action for TLR3-moDC participation in the inflammatory cascade to disease. Previously, we and subsequently many others proposed that airway inflammatory disease was initiated by a primary response from sentinel epithelial cells that are the first to respond to inhaled stimuli with endogenous danger signals such as CCL5, IL-33, and mitogen-activated protein kinase 13 (7, 8, 16). Activation of TLR3 has proven difficult to track, however, the tight link between viral replication (providing dsRNA) and TLR3 expression suggests that expression can be a measure of functional activation in vivo. In any case, the transient nature of TLR3 expression makes unlikely that TLR3 manifests chronic

activation to explain a persistent drive for inflammatory disease. Relevant to this issue, endogenous RNA from ongoing cell turnover and/or necrosis might also activate TLR3 signaling (57–59) but this issue still needs to be established in the context of viral injury and subsequent repair. In support of another long-lasting mechanism, others have shown that SeV vectors can also provide a persistent signal for moDC maturation in the setting of long-term immunotherapy (60), perhaps similar to the present observations. In either case, the nature of endosomal TLR3 activation suggests that immune cell participation depends on a transient signal that is endogenous to virus-infected moDCs. However, it is also possible that other virus-infected cells (e.g., lung epithelial cells) could provide a signal to moDCs for accumulation (via cell recruitment or survival) and activation at the site of disease (9, 16). Others have separated mouse lung DCs into cDC1 and cDC2 populations that correspond to $CD11b^+$ DC and $CD103^+$ DC populations, as well as an inflammatory cDC2 population that correspond to a subset of our $CD11b^+$ DC population (61). Thus, the present approach excludes these subsets from the moDC population that drives post-viral lung disease in the present model. These findings are consistent with the development of post-viral disease without a detectable contribution from conventional T cells that might be activated by non-moDC populations (6).

These issues raise the fifth aspect of our findings and the consequent proposal for reprogramming of lung epithelial cells, and in particular epithelial stem cells, that might explain persistent progression and susceptibility to lung disease. In that regard, we found that moDC-TLR3 function was required for the expansion of the AT2 cell population, which in the mouse is likely the primary site of IL-33 expression versus airway basal cells as the epithelial site in humans (8, 11, 22–24). In both cases, this epithelial cell expansion could therefore drive a downstream type 2 immune response characterized by increased IL-13 production and IL-13-stimulated inflammation and mucus production. Notably, the same epithelial cell expansion is also found after infection with other respiratory viruses including SARS-CoV-2 in animal models (mice, hamsters, and monkeys) and human autopsies (15, 62–64) as a potential pathway to post-viral disease. Similarly, as introduced above, others have shown that TLR3 function is required for maintenance of epithelial barrier function in the airway (42) and repair of the epithelial barrier after UV-damage in the skin (65) and irradiation-induced damage in the gut (66). Other studies suggest that TLR3 could contribute to this epithelial effect via cytokine-signaling such as activation of IL-6-STAT3 (59) and/or an epigenetic alteration such as the gene-specific chromatin modification as found for activation of TLR4 (67). However, these observations derive from studies of stromal cells, and the mechanism requiring immune cells such as moDCs still needs to be defined. In that regard, one report found defective wound healing in TLR3-deficient mice that was associated with poor recruitment of myeloid cells, but this effect was short-term and TRIF-dependent (68). Thus, further study will need to define the pathway for the TLR3-moDC combination to drive a persistent and excessive epithelial cell response after viral infection that is independent of TRIF signaling.

As introduced above, the sixth impact of our study is the implication for human diseases. Thus, the same bronchoalveolar pattern of disease is found after infections with other common respiratory viruses, including SARS-CoV-1 (69) and SARS-CoV-2 (63), when the viral receptor is endogenous (using species-adapted virus or naturally-susceptible species).

In cases where the receptor is expressed via vector or transgenic methods, histopathology manifests instead primarily in the site of expression, e.g., alveolar epithelial cells (62, 70). In all cases, however, there is an alveolar epithelial repair process that depends on AT2 cell expansion derived from proliferation and differentiation of epithelial stem cells (ESCs), as exemplified by infections with influenza A virus in mice (21, 71) and SARS-CoV-2 in humans (15). The present results indicate that the AT2 stem cell expansion might depend on viral activation of the TLR3-moDC component of the immune response and therefore might trigger a self-renewing process that allows for progression to long-term lung disease. Human studies already suggest that this type of disease pathway is also activated in chronic lung diseases such as asthma and COPD that are subject to initiation, exacerbation, and progression after respiratory viral infection (4). The present identification of the TLR3-moDC immune component in the epithelial response to injury therefore provides another diagnostic and therapeutic target for correcting an excessive inflammatory response and thereby attenuating post-viral lung disease. Indeed, TLR3 itself has been targeted with small molecular-weight molecules (66, 72) and antibodies to block TLR3-dependent signal transduction (52, 58, 73, 74). However, the small molecule that was selected suffers from uncertain pharmacokinetic properties in vivo, and the anti-TLR3 Ab might not be effective if it does not reach the preferred intracellular (often endosomal) location of TLR3 in dendritic cells versus stromal cells (51). Indeed, our analysis of TLR3 expression using flow cytometry (as shown in Fig. 5) required cell permeabilization for TLR3 detection (as described in Methods and Materials). Therefore, intracellular localization of TLR3 might contribute to the poor efficacy found in the clinical trial of anti-TLR3 mAb in human rhinovirus-challenge in asthma patients (74). Similarly, there also needs to be precise assays of TLR3 expression/activation to follow target behavior. These pursuits and related strategies to limit epithelial stem cell activation to the initial repair phase will be productive based on the present model of post-viral lung disease.

Together, the present results provide for several general and specific concepts for understanding and controlling long-term and often progressive inflammatory lung disease after respiratory viral infection. General concepts include: (1) a front-line immune cell niche instead of the generally proposed sentinel epithelial cell population as the initial trigger for virus-induced disease; (2) the selective nature of TLR3 activation and moDC participation in this niche instead of the usual downstream effector role for immune cells in inflammation; (3) the trophic action of $TLR3^{+}$ moDCs to expand the lung epithelial cell population as a source of IL-33 that is required to drive a downstream type 2 immune response versus previous reliance on other types of immune cells such as ILC2s, M2-macrophages, and eosinophils. These elements provide a revised scheme (as depicted in Fig. 11) that translates to the likelihood of early and transient activation of the innate immune response can switch the host to a long-lasting disease pathway. The progressive and chronic nature of the disease process is distinct from short-term role of TLR3 (or other pathogen recognition receptors) in inflammation (38–40, 75–78) and dendritic cell maturation after viral infection (60, 79). The alternative dendritic-epithelial cell interface still needs to be fully defined, but the present evidence already offers the likelihood that this site can reprogram an epithelial stem cell subset from useful repair of injury to an excessive proliferative/survival response with consequences for downstream inflammation, mucus production, and remodeling in the lung.

The present results thereby provide an additional checkpoint for correcting the progressive disease that can develop after respiratory viral infections.

Acknowledgments

The authors thank Lora Benoit, Di Wu, Xiaohua Jin, Chaeho Park, Rose Tidwell, Yingjian You, and the staff in the Siteman Flow Cytometry Core and Pulmonary Morphology Core at Washington University for outstanding advice and technical support.

This work was supported by grants from the National Institute of Allergy and Infectious Diseases (R01 AI130591) and National Heart, Lung, and Blood Institute (R35 HL145242), the Cystic Fibrosis Foundation, and the Hardy Trust and Schaeffer Funds.

Abbreviations used in this article:

AT2 cell	alveolar epithelial type 2 cell
ATCC	American Type Culture Collection
BMDC	bone-marrow-derived dendritic cells
COPD	chronic obstructive pulmonary disease
IAV	influenza A virus
ILC2	group 2 innate lymphoid cell
NP	nucleoprotein
PAS	periodic acid-Schiff
qPCR	quantitative PCR
moDC	monocyte-derived dendritic cell
Muc5ac	mucin 5AC
SeV	Sendai virus
Sftpc	surfactant protein C
TRIF	TIR-domain-containing adapter-inducing IFN-β

References

1. Holtzman MJ, Morton JD, Shornick LP, Tyner JW, O'Sullivan MP, Antao A, Lo M, Castro M, and Walter MJ. 2002. Immunity, inflammation, and remodeling in the airway epithelial barrier: epithelial-viral-allergic paradigm. Physiol. Rev 82: 19–46. [PubMed: 11773608]
2. Holtzman MJ, Patel D, Zhang Y, and Patel AC. 2011. Host epithelial-viral interactions as cause and cure for asthma. Curr. Opin. Immunol 23: 487–494. [PubMed: 21703838]
3. Holtzman MJ 2012. Asthma as a chronic disease of the innate and adaptive immune systems responding to viruses and allergens. J. Clin. Invest 122: 2741–2748. [PubMed: 22850884]
4. Holtzman MJ, Byers DE, Alexander-Brett J, and Wang X. 2014. The role of airway epithelial cells and innate immune cells in chronic respiratory disease. Nat. Rev. Immunol. 14: 686–698. [PubMed: 25234144]

5. Tyner JW, Kim EY, Ide K, Pelletier MR, Roswit WT, Morton JD, Battaile JT, Patel AC, Patterson GA, Castro M, Spoor MS, You Y, Brody SL, and Holtzman MJ. 2006. Blocking airway mucous cell metaplasia by inhibiting EGFR antiapoptosis and IL-13 transdifferentiation signals. J. Clin. Invest 116: 309–321. [PubMed: 16453019]
6. Kim EY, Battaile JT, Patel AC, You Y, Agapov E, Grayson MH, Benoit LA, Byers DE, Alevy Y, Tucker J, Swanson S, Tidwell R, Tyner JW, Morton JD, Castro M, Polineni D, Patterson GA, Schwendener RA, Allard JD, Peltz G, and Holtzman MJ. 2008. Persistent activation of an innate immune response translates respiratory viral infection into chronic lung disease. Nat. Med 14: 633–640. [PubMed: 18488036]
7. Alevy Y, Patel AC, Romero AG, Patel DA, Tucker J, Roswit WT, Miller CA, Heier RF, Byers DE, Brett TJ, and Holtzman MJ. 2012. IL-13–induced airway mucus production is attenuated by MAPK13 inhibition. J. Clin. Invest 122: 4555–4568. [PubMed: 23187130]
8. Byers DE, Alexander-Brett J, Patel AC, Agapov E, Dang-Vu G, Jin X, Wu K, You Y, Alevy YG, Girard J-P, Stappenbeck TS, Patterson GA, Pierce RA, Brody SL, and Holtzman MJ. 2013. Long-term IL-33-producing epithelial progenitor cells in chronic obstructive lung disease. J. Clin. Invest 123: 3967–3982. [PubMed: 23945235]
9. Wu K, Byers DE, Jin X, Agapov E, Alexander-Brett J, Patel AC, Cella M, Gilfilan S, Colonna M, Kober DL, Brett TJ, and Holtzman MJ. 2015. TREM-2 promotes macrophage survival and lung disease after respiratory viral infection. J. Exp. Med 212: 681–697. [PubMed: 25897174]
10. Zhang Y, Mao D, Keeler SP, Wang X, Wu K, Gerovac BJ, Shornick LP, Agapov E, and Holtzman MJ. 2019. Respiratory enterovirus (like parainfluenza virus) can cause chronic lung disease if protection by airway epithelial STAT1 is lost. J. Immunol. 202: 2332–2347. [PubMed: 30804041]
11. Wu K, Wang X, Keeler SP, Gerovac BJ, Agapov E, Byers DE, Gilfillan S, Colonna M, Zhang Y, and Holtzman MJ. 2020. Group 2 innate lymphoid cells must partner with the myeloid-macrophage lineage for long-term postviral lung disease. J Immunol 205: 1084–1101. [PubMed: 32641386]
12. Agapov E, Battaile JT, Tidwell R, Hachem R, Patterson GA, Pierce RA, Atkinson JJ, and Holtzman MJ. 2009. Macrophage chitinase 1 stratifies chronic obstructive lung disease. Am. J. Respir. Cell Mol. Biol 41: 379–384. [PubMed: 19491341]
13. Byers DE, Wu K, Dang-Vu G, Jin X, Agapov E, Zhang X, Battaile JT, Schechtman KB, Yusen R, Pierce RA, and Holtzman MJ. 2018. Triggering receptor expressed on myeloid cells-2 (TREM-2) expression tracks with M2-like macrophage activity and disease severity in COPD. Chest 153: 77–86. [PubMed: 29017955]
14. Keeler SP, Agapov EV, Hinojosa ME, Letvin AN, Wu K, and Holtzman MJ. 2018. Influenza A virus infection causes chronic lung disease linked to sites of active viral RNA remnants. J. Immunol. 201: 2354–2368. [PubMed: 30209189]
15. Chen J, Wu H, Yu Y, and Tang N. 2020. Pulmonary alveolar regeneration in adult COVID-19 patients. Cell Research 30: 708–710. [PubMed: 32632255]
16. Tyner JW, Uchida O, Kajiwara N, Kim EY, Patel AC, O'Sullivan MP, Walter MJ, Schwendener RA, Cook DN, Danoff TM, and Holtzman MJ. 2005. CCL5-CCR5 interaction provides antiapoptotic signals for macrophage survival during viral infection. Nat. Med 11: 1180–1187. [PubMed: 16208318]
17. Bosurgi L, Cao YG, Cabeza-Cabrerizo M, Tucci A, Hughes LD, K. Y, Weinstein JS, Licona-Limon P, Schmid ET, Pelorosso F, Gagliani N, Craft JE, Flavell RA, Ghosh S, and Rothlin CV. 2017. Macrophage function in tissue repair and remodeling requires IL-4 or IL-13 with apoptotic cells. Science 356.
18. Gieseck RL, Wilson MS, and Wynn TA. 2017. Type 2 immunity in tissue repair and fibrosis. Nat. Rev. Immunol in press.
19. Lechner AJ, Driver IH, Lee J, Conroy CM, Nagle A, Locksley RM, and Rock JR. 2017. Recruited monocytes and type 2 immunity promote lung regeneration following pneumonectomy. Cell Stem Cell 21: 120–134. [PubMed: 28506464]
20. Hung L-Y, Sen D, Oniskey TK, Katzen J, Cohen NA, Vaughan AE, Nieves W, Urisman A, Beers MF, Krummel MF, and Herbert DR. 2018. Macrophages promote epithelial proliferation following infectious and non-infectious lung injury through a Trefoil factor 2-dependent mechanism. Mucosal immunology 12: 64–76. [PubMed: 30337651]

21. Zacharias WJ, Frank DB, Zepp JA, Morley MP, Alkhaleel FA, Kong J, Zhou S, Cantu E, and Morrisey EE. 2018. Regeneration of the lung alveolus by an evolutionarily conserved epithelial progenitor. Nature 555: 251–255. [PubMed: 29489752]
22. Hardman CS, Panova V, and McKenzie ANJ. 2012. IL-33 citrine reporter mice reveal the temporal and spatial expression of IL-33 during allergic lung inflammation. Eur. J. Immunol 43: 1–11.
23. Pichery M, Mirey E, Mercier P, Lefrancais E, Dujardin A, Ortega N, and Girard J-P. 2012. Endogenous IL-33 is highly expressed in mouse epithelial barrier tissues, lymphoid organs, brain, embryos, and inflamed tissues: in situ analysis using a novel Il-33-LacZ gene trap reporter strain. J. Immunol 188: 3488–3495. [PubMed: 22371395]
24. Mohapatra A, Van Dyken SJ, Schneider C, Nussbaum JC, Liang H-E, and Locksley RM. 2016. Group 2 innate lymphoid cells utilize the IRF4-IL-9 module to coordinate epithelial cell maintenance of lung homeostasis. Mucosal immunology 9: 275–286. [PubMed: 26129648]
25. Alexopoulou L, Holt AC, Medzhitov R, and Flavell RA. 2001. Recognition of double-stranded RNA and activation of NF-kappaB by Toll- like receptor 3. Nature 413: 732–738. [PubMed: 11607032]
26. Walter MJ, Kajiwara N, Karanja P, Castro M, and Holtzman MJ. 2001. IL-12 p40 production by barrier epithelial cells during airway inflammation. J. Exp. Med 193: 339–352. [PubMed: 11157054]
27. Livak KJ, and Schmittgen TD. 2001. Analysis of relative gene expression data using real-time quantitative PCR and the 2(-Delta Delta C(T)) Method. Methods 25: 402–408. [PubMed: 11846609]
28. van Rijt LS, Jung S, Kleinjan A, Vos N, Willart M, Duez C, Hoogsteden HC, and Lambrecht BN. 2005. In vivo depletion of lung CD11c+ dendritic cells during allergen challenge abrogates the characteristic features of asthma. J. Exp. Med 201: 981–991. [PubMed: 15781587]
29. Grayson MH, Cheung D, Rohlfing MM, Kitchens R, Spiegel DE, Tucker J, Battaile JT, Alevy Y, Yan L, Agapov E, Kim EY, and Holtzman MJ. 2007. Induction of high-affinity IgE receptor on lung dendritic cells during viral infection leads to mucous cell metaplasia. J. Exp. Med 204: 2759–2769. [PubMed: 17954569]
30. Inaba K, Inaba M, Romani N, Aya H, Deguchi M, Ikehara S, Muramatsu S, and Steinman RM. 1992. Generation of large numbers of dendritic cells from mouse bone marrow cultures supplemented with granulocyte/macrophage colony-stimulating factor. J. Exp. Med 176: 1693–1702. [PubMed: 1460426]
31. Aegerter H, Kulikauskaite J, Crotta S, Patel H, Kelly G, Hessel EM, Mack M, Beinke S, and Wack A. 2020. Influenza-induced monocyte-derived alveolar macrophages confer prolonged antibacterial protection. Nat. Immunol 21: 145–157. [PubMed: 31932810]
32. Walter MJ, Morton JD, Kajiwara N, Agapov E, and Holtzman MJ. 2002. Viral induction of a chronic asthma phenotype and genetic segregation from the acute response. J. Clin. Invest 110: 165–175. [PubMed: 12122108]
33. Yamamoto M, Sato S, Hemmi H, Hoshino H, Kaisho T, Sanjo H, Takeuchi K, Sugiyama M, Okabe M, Takeda K, and Akira S. 2003. Role of adaptor TRIF in the MyD88-independent Toll-like receptor signaling pathway. Science 301: 640–643. [PubMed: 12855817]
34. Hoebe K, Du K, Georgel P, Janssen E, Tabeta K, Kim SO, Goode J, Lin P, Mann N, Mudd S, Crozat K, Sovath S, Han J, and Beutler B. 2003. Identification of Lps2 as a key transducer of MyD88-independent TIR signaling. Nature 424: 743–748. [PubMed: 12872135]
35. Ueda A, Okuda K, Ohno S, Shirai A, Igarashi T, Matsunaga K, Fukushima J, Kawamoto s., Ishigatsubo Y, and Okubo T. 1994. NF-kappa B nd Sp1 regulate transcription of the human monocyte chemoattractant protein-1 gene. J. Immunol 1994: 2052–2063.
36. Desch AN, Randolph GJ, Murphy KM, Gautier EL, Kedl RM, Lahoud MH, Caminschi I, Shortman K, Henson PM, and Jakubzick CV. 2011. CD103+ pulmonary dendritic cells preferentially acquire and present apoptotic cell-associated antigen. J. Exp. Med 208: 1789–1797. [PubMed: 21859845]
37. Jin D, and Sprent J. 2018. GM-CSF culture revisited: preparation of bulk populations of highly pure dendritic cells from mouse bone marrow. J. Immunol 201: 3129–3139. [PubMed: 30322963]

38. Wang Q, Miller DJ, Bowman ER, Nagarkar DR, Schneider D, Zhao Y, Linn MJ, Goldsmith AM, Bentley JK, Sajjan US, and Hershenson MB. 2011. MDA5 and TLR3 initiate pro-inflammatory signaling pathways leading to rhinovirus-induced airways inflammation and hyperresponsiveness. PLoS Pathog 7: e1002070. [PubMed: 21637773]
39. Le Goffic R, Balloy V, Lagranderie M, Alexopoulou L, Escriou N, Flavell RA, Chignard M, and Si-Tahar M. 2006. Detrimental contribution of the Toll-like receptor (TLR)3 to influenza A virus-induced acute pneumonia. PLoS Pathog 2: e53. [PubMed: 16789835]
40. Rudd BD, Smit JJ, Flavell RA, Alexopoulou L, Schaller MA, Gruber A, Berlin AA, and Lukacs NW. 2006. Deletion of TLR3 alters the pulmonary immune environment and mucus production during respiratory syncytial virus infection. J. Immunol 176: 1937–1942. [PubMed: 16424225]
41. Gitlin L, Benoit LA, Song C, Cella M, Gilfilan S, Holtzman MJ, and Colonna M. 2010. Melanoma differentiation-associated gene 5 (MDA5) is involved in the innate immune response to Paramyxoviridae infection in vivo. PLoS Pathog 6: e10000734.
42. Veazey JM, Chapman TJ, Smyth TR, Hillman SE, Eliseeva SI, and Georas SN. 2019. Distinct roles for MDA5 and TLR3 in the acute response to inhaled double-stranded RNA. PloS ONE 14: e0216056. [PubMed: 31067281]
43. Shornick LP, Wells AG, Zhang Y, Patel AC, Huang G, Takami K, Sosa M, Shukla NA, Agapov E, and Holtzman MJ. 2008. Airway epithelial versus immune cell Stat1 function for innate defense against respiratory viral infection. J. Immunol 180: 3319–3328. [PubMed: 18292557]
44. Melchjorsen J, Jensen SB, Malmgaard L, Rasmussen SB, Weber F, Bowie AG, Matikainen S, and Paludan SR. 2005. Activation of innate defense against a paramxyovirus is mediated by RIG-I and TLR7 and TLR8 in a cell-type-specific manner. J. Virol 79: 12944–12951. [PubMed: 16188996]
45. Zhang S-Y, Herman M, Ciancanelli MJ, Perez de Diego R, Sancho-Shimizu V, Abel L, and Casanova J-L. 2013. TLR3 immunity to infection in mice and humans. Curr Opin Immunol 25: 19–33. [PubMed: 23290562]
46. Totura AL, Whitmore A, Agnihothram S, Schafer A, Katze MG, Heise MT, and Baric RS. 2020. Toll-like receptor 3 signaling via TRIF contributes to a protective immune response to severe acute repiratory syndrome coronavirus infection. mBio 6: e00638–00615.
47. Yamashita M, Chattopadhyay S, Fensterl V, Zhang Y, and Sen GC. 2012. A TRIF-independent branch of TLR3 signaling. J. Immunol 188: 2825–2833. [PubMed: 22323545]
48. Zhu L, Lee P, Lee W, Zhao Y, Yu D, and Chen Y. 2009. Rhinovirus-induced major airway mucin production involves a novel TLR3-EGFR-dependent pathway. Am J Respir Cell Mol Biol 40: 610–619. [PubMed: 18978302]
49. Patel AC, Morton JD, Kim EY, Alevy Y, Swanson S, Tucker J, Huang G, Agapov E, Phillips TE, Fuentes ME, Iglesias A, Aud D, Allard JD, Dabbagh K, Peltz G, and Holtzman MJ. 2006. Genetic segregation of airway disease traits despite redundancy of chloride channel calcium-activated (CLCA) family members. Physiol. Genomics 25: 502–513. [PubMed: 16569774]
50. Torres DA, Dieudonne A, Ryffel B, Vilain E, Si-Tahar M, Pichavant M, Lassalle P, Trottein F, and Gosset P. 2010. Double-stranded RNA exacerbates pulmonary allergic reaction through TLR3: implication of airway epithelium and dendritic cells. J. Immunol 185: 451–459. [PubMed: 20505141]
51. Matsumoto M, Funami K, Tanabe M, Oshiumi H, Shingai M, Seto Y, Yamamoto A, and Seya T. 2003. Subcellular localization of Toll-like receptor 3 in human dendritic cells. J. Immunol 171: 3154–3162. [PubMed: 12960343]
52. Murakami Y, Fukui R, Motoi Y, Kanno A, Shibata T, Tanimura N, Saitoh S, and Miyake K. 2014. Roles of cleaved N-terminal TLR3 fragment and cell surface TLR3 in double-stranded RNA sensing. J. Immunol 193: 5208–5217. [PubMed: 25305318]
53. Bhargava P, Nogueras-Ortiz C, Chawla S, Baek R, Moller Jorgensen M, and Kapogiannis D. 2019. Altered levels of Toll-like receptors in circulating extracellular vesicles in multiple sclerosis. Cells 8: 1058.
54. Mills JT, Schwenzer A, Marsh EK, Edwards MR, Sabroe I, Midwood KS, and Parker LC. 2019. Airway epithelial cells generate pro-inflammatory tenascin-C and small extracellular vesicles in response to TLR3 stimuli and rhinovirus infection. Front Immunol 10: 1–12. [PubMed: 30723466]

55. Plantinga M, Guilliams M, Vanheerswyngheis M, Deswarte K, Branco-Madeira F, Toussaint W, Vanhoutte L, Neyt K, Killeen N, Malissen B, Hammad H, and Lambrecht BN. 2013. Conventional and monocyte-derived CD11b+ dendritic cells initiate and maintain T helper cell-mediated immunity to house dust mite allergene. Immunity 38: 322–335. [PubMed: 23352232]

56. Grayson MH, Ramos MS, Rohlfing MM, Kitchens R, Wang HD, Gould A, Agapov E, and Holtzman MJ. 2007. Controls for lung dendritic cell maturation and migration during respiratory viral infection. J. Immunol 179: 1438–1448. [PubMed: 17641009]

57. Kariko K, Ni H, Capodici J, Lamphier M, and Weissman D. 2004. mRNA is an endogenous ligand for Toll-like receptor 3. J. Biol. Chem 279: 12542–12550. [PubMed: 14729660]

58. Cavassani KA, Ishii M, Wen H, Schaller MA, Lincoln PM, Lukacs NW, Hogaboam CM, and Kunkel SL. 2008. TLR3 is an endogenous sensor of tissue necrosis during acute inflammatory events. J. Exp. Med 205.

59. Nelson AM, Reddy SK, Ratliff TS, Hossain MZ, Katseff AS, Zhu AS, Chang E, Resnik s. R., Page C, Kim DS, Whittam AJ, Miller LS, and Garza LA. 2015. dsRNA released by tissue damage activates TLR3 to drive skin regeneration. Cell Stem Cell 17: 139–151. [PubMed: 26253200]

60. Okano S, Yonemitsu Y, Shirabe K, Kakeji Y, Maehara Y, Harada M, Yoshikai Y, Inoue M, Hasegawa, and Sueishi K. 2011. Provision of continuous maturation signaling to dendritic cells by RIG-I-stimulting cytosolic RNA synthesis of Sendai virus. J. Immunol 186: 1828–1839. [PubMed: 21187441]

61. Bosteels C, Neyt K, Vanheerswynghels M, van Helden MJ, Sichien D, Debeuf N, De Prijck S, Bosteels V, Vandamme N, Martens L, Saeys Y, Louagie E, Lesage M, Willliams DL, Tang S-C, Mayer JU, Ronchese F, Scott CL, Hammad H, Guilliams M, and Lambrecht BN. 2020. Inflammatory type 2 cDCs acquire features of cDC1s and macrophages to orchestrate immunity to respiratory virus infection. Immunity 52: 1039–1056. [PubMed: 32392463]

62. Winkler ES, Bailey AL, Kafai NM, Nair S, McCune BT, Yu J, Fox JM, Chen RE, Earnest JT, Keeler SP, Ritter JH, Kang L-I, Dort S, Robichaud A, Head RD, Holtzman MJ, and Diamond MS. 2020. SARS-CoV-2 infection in the lungs of human ACE2 transgenic mice causes severe inflammation and immune cell infiltration and compromised respiratory function. Nat. Immunol in press.

63. Sia SF, Yan L-M, Chin AWH, Fung K, Choy K-T, Wong AYL, Kaewpreedee P, Perera RAPM, Poon LLM, Nicholls JM, Peiris M, and Yen H-L. 2020. Pathogenesis and transmission of SARS-CoV-2 in golden hamsters. Nature 583: 834–838. [PubMed: 32408338]

64. Munster VJ, Feldmann F, Williamson BN, van Doremalen N, Perez-Perez L, Schulz J, Meade-White K, Okumura A, Callison J, Brumbaugh B, Avanzato VA, Rosenke R, Hanley PW, Saturday G, Scott D, Fischer ER, and de Wit E. 2020. Respiratory disease and virus shedding in rhesus macaques inoculated with SARS-CoV-2. bioRxiv in press.

65. Borkowski AW, Kuo I-S, Bernard JJ, Yoshida T, Williams MR, Hung N-J, Yu BD, Beck LA, and Gallo RL. 2015. Toll-like receptor 3 activation is required for normal skin barrier repair following UV damage. J. Invest. Dermatol 135: 569–578. [PubMed: 25118157]

66. Takemura N, Kawasaki T, Kunisawa J, Sato S, Lamichhane A, Kobiyama K, Aoshi T, Ito J, Mizuguchi K, Karuppuchamy T, Matsunaga K, Miyatake S, Mori N, Tsujimura T, Satoh T, Kumagai Y, Kawai T, Standley DM, Ishii KJ, Kiyono H, Akira S, and Uematsu S. 2014. Blockade of TLR3 protects mice from lethal radiation-induced gastrointestinal syndrome. Nat. Comm 5: 3492.

67. Foster SL, Hargreaves DC, and Medzhitov R. 2007. Gene-specific control of inflammation by TLR-induced chromatin modifications. Nature 447: 972–978. [PubMed: 17538624]

68. Lin Q, Fang D, Fang J, Ren X, Yang X, Wen F, and Su SB. 2011. Impaired wound healing with defective expression of chemokines and recruitment of myeloid cells in TLR3-deficient mice. J. Immunol 186: 3710–3717. [PubMed: 21317384]

69. Page C, Goicochea L, Matthews K, Zhang Y, Klover P, Holtzman MJ, Hennighausen L, and Frieman M. 2012. Induction of alternatively activated macrophages enhances pathogenesis during severe acute respriatory syndrome coronavirus infection. J. Virol 86: 13334–13349. [PubMed: 23015710]

70. Hassan AO, Case JB, Winkler ES, Thackray LB, Kafai NM, Bailey AL, McCune BT, Fox JM, Chen RE, Alsoussi WB, Tumer JS, Schmitz AM, Lei T, Shrihari S, Keeler SP, Fremont DH, Greco

S, McCray PBJ, Perlman S, Holtzman MJ, Ellebedy AH, and Diamond MS. 2020. A SARS-CoV-2 infection model in mice demonstrates protection by neutralizing antibodies. Cell 182: in press.

71. Kumar PA, Hu Y, Yamamoto Y, Hoe NB, Wei TS, Mu D, Sun Y, Joo LS, Dagher R, Zielonka EM, Wang DY, Lim B, Chow VT, Crum CP, Xian W, and McKeon F. 2011. Distal airway stem cells yield alveoli in vitro and during lung regeneration following H1N1 influenza infection. Cell 147: 525–538. [PubMed: 22036562]
72. Cheng K, Wang X, and Yin H. 2011. Small-molecule inhibitors of the TLR3/dsRNA complex. J. Am. Chem. Soc 133: 3764–3767. [PubMed: 21355588]
73. Bunting RA, Duffy KE, Lamb RJ, San Mateo LR, Smalley K, Raymond H, Liu X, Petley T, Fisher J, Beck H, Flavell RA, Alexopoulou L, and Ward CK. 2011. Novel antagonist antibody to TLR3 blocks poly(I:C)-induced inflammation in vivo and in vitro. Cell. Immunol 267: 9–16. [PubMed: 21092943]
74. Silkoff PE, Flavin S, Gordon R, Loza MJ, Sterk PJ, Lutter R, Diamant Z, Turner RB, Lipworth BJ, Proud D, Singh D, Eich A, Backer V, Gern JE, Herzmann C, Halperin SA, Mensigna TT, Del Vecchio AM, Branigan P, San Mateo L, Baribaud F, Barnathan ES, and Johnston SL. 2017. Toll-like receptor 3 blockade in rhinovirus-induced experimental asthma exacerbations: a randomized controlled study. J. Allergy Clin. Immunol in press.
75. Wang T, Town T, Alexopoulou L, Anderson JF, Fikrig E, and Flavell RA. 2004. Toll-like receptor 3 mediates West Nile virus entry into the brain causing lethal encephalitis. Nat. Med 10: 1366–1373. [PubMed: 15558055]
76. Gowen BB, Hoopes JD, Wong MH, Jung KH, Isakson KC, Alexopoulou L, Flavell RA, and Sidwell RW. 2006. TLR3 deletion limits mortality and disease severity due to Phlebovirus infection. J. Immunol 177: 6301–6307. [PubMed: 17056560]
77. Hutchens M, Luker ME, Sottile P, Sonstein J, Lukacs NW, Nune G, Curtis JL, and Luker GD. 2008. TLR3 increases disease morbidity and mortality from vaccinia infection. J. Immunol. 180: 483–491. [PubMed: 18097050]
78. Lukacs NW, Smit JJ, Mukherjee S, Morris SB, Nunez G, and Lindell DM. 2010. Respiratory virus-induced TLR7 activation controls IL-17 associated increased mucus via IL-23 regulation. J. Immunol 185: 2231–2239. [PubMed: 20624950]
79. Lopez CB, Moltedo B, Alexopoulou L, Bonifaz L, Flavell RA, and Moran TM. 2004. TLR-independent induction of dendritic cell maturation and adaptive immunity by negative-strand RNA viruses. J. Immunol 173: 6882–6889. [PubMed: 15557183]

Key points:

1. Activation of TLR3$^+$ moDCs predominates after respiratory viral infection.
2. TLR3 and moDCs are required for progressive post-viral lung disease.
3. TLR3$^+$ moDCs expand lung epithelial cells that are key to post-viral disease.

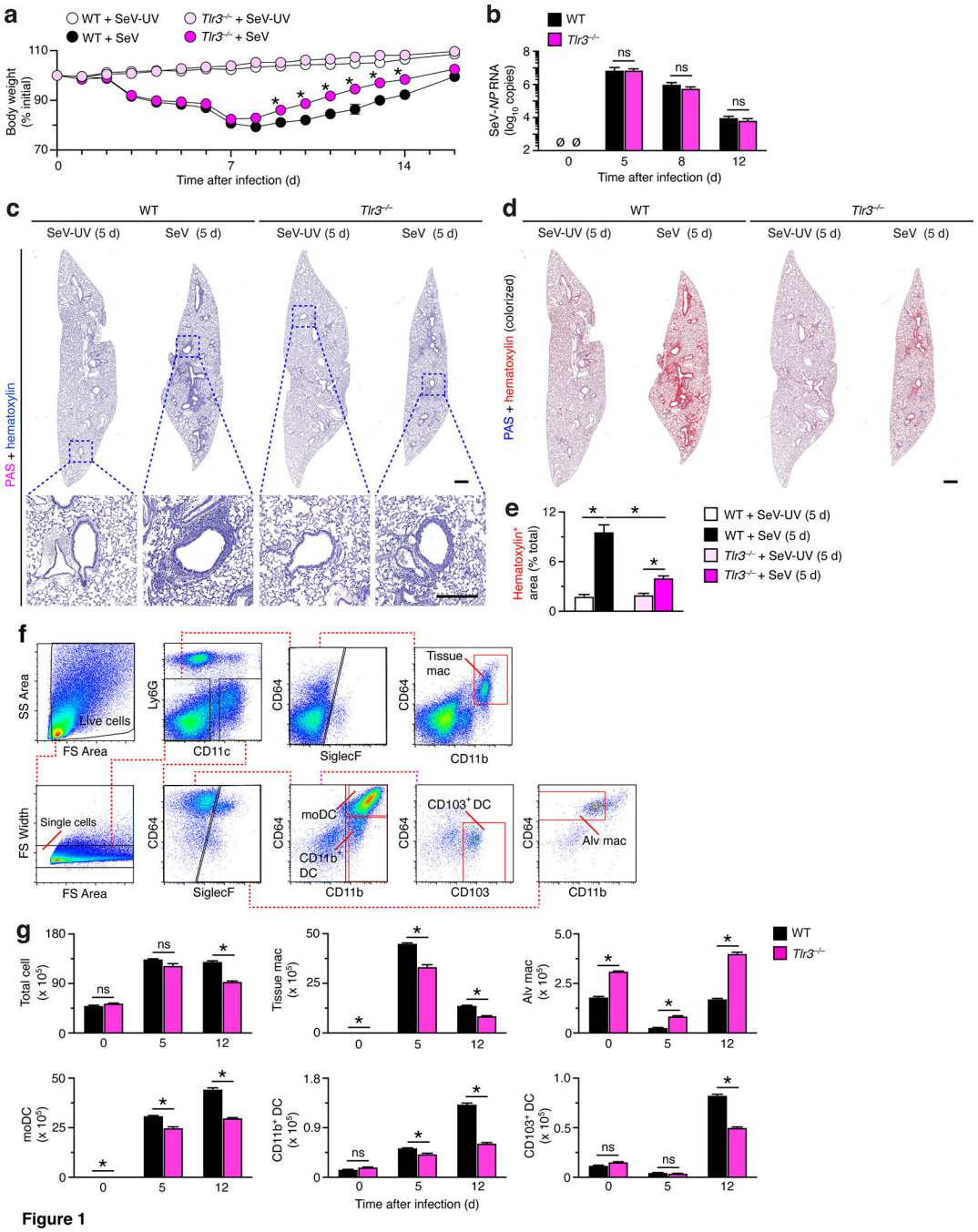

Figure 1

FIGURE 1.

TLR3-deficiency attenuates acute inflammatory illness after viral infection. (**a**) Body weights from wild-type (WT) and *Tlr3*$^{-/-}$ mice after infection with SeV or control SeV-UV. (**b**) Levels of SeV *NP* RNA in lungs from WT and *Tlr3*$^{-/-}$ mice after infection with SeV. (**c**) PAS and hematoxylin staining of lung sections from WT and *Tlr3*$^{-/-}$ mice at 5 d after SeV or SeV-UV. Small scale bar, 500 μm; large scale bar, 250 μm. (**d**) Lung sections from (c) with hematoxylin staining colorized red using image analysis. (**e**) Quantification of red colorized staining from (d). (**f**) Flow cytometry analysis of tissue macrophage (Ly6G^{-}CD11c^{-}Siglec-

F^{-}F4/80^{+}CD11b^{+}), alveolar macrophage (Ly6G^{-}CD11c^{+}Siglec-F^{+}F4/80^{+}CD11b^{-}), moDC (Ly6G^{-}CD11c^{+}Siglec-F^{-}CD64^{+}CD11b^{+}), CD103^{+} DC (Ly6G^{-}CD11c^{+}Siglec-F^{-}CD64^{+}CD11b^{-}CD103^{+}), and CD11b^{+} DC (Ly6G^{-}CD11c^{+}Siglec-F^{-}CD64CD11b^{+}) populations in lung tissue from WT mice at 12 d after SeV infection. (**g**) Flow cytometry-based levels of total and immune cell populations in lung tissue from WT and *Tlr3*$^{-/-}$ mice at indicated timepoints after SeV infection using conditions in (f). All data are representative of three separate experiments (mean and SEM) with at least 5 mice per condition in each experiment. *P<0.01.

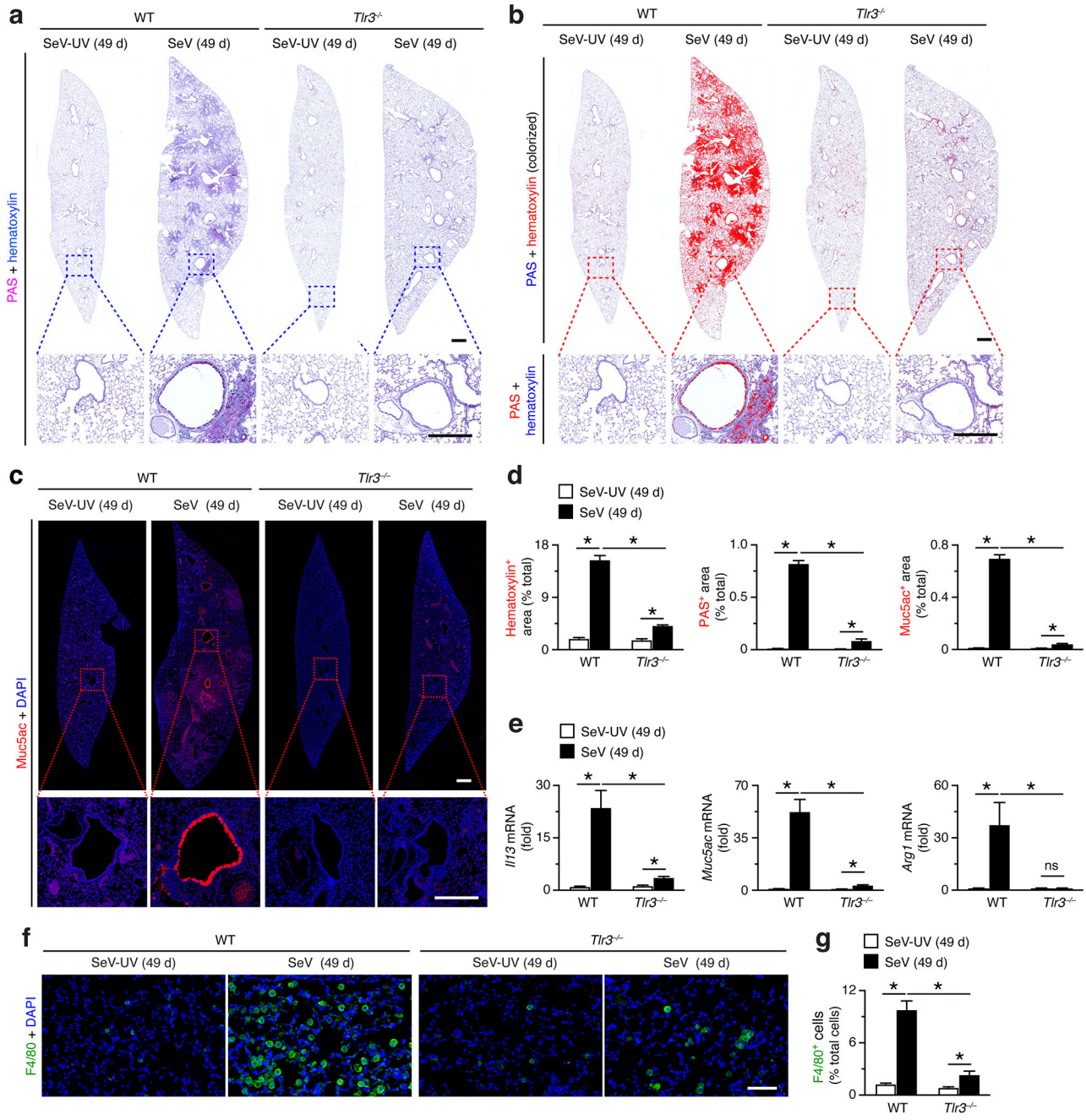

Figure 2

FIGURE 2.

TLR3-deficiency attenuates chronic lung disease after viral infection. (**a**) PAS and hematoxylin staining of lung sections from WT and *Tlr3*$^{-/-}$ mice at 49 d after SeV infection or SeV-UV. Small scale bar, 500 μm; large scale bar, 250 μm. (**b**) Lung sections from (a) with hematoxylin and PAS staining colorized red with image analysis. (**c**) Muc5ac immunostaining of lungs for conditions in (a). Small scale bar, 500 μm; large scale bar, 250 μm. (**d**) Quantification of red-colorized staining from (b) and immunostaining from (c). (**e**) Levels of *Il13*, *Muc5ac*, and *Arg1* mRNA in lungs from WT and *Tlr3*$^{-/-}$ mice at 49 d after

SeV infection or SeV-UV. (**f**) F4/80 immunostaining of lung sections for conditions in (a). Scale bar, 200 μm. (**g**) Quantification of immunostaining from (f). All data are representative of three separate experiments (mean and SEM) with at least 5 mice per condition in each experiment. *$P<0.01$.

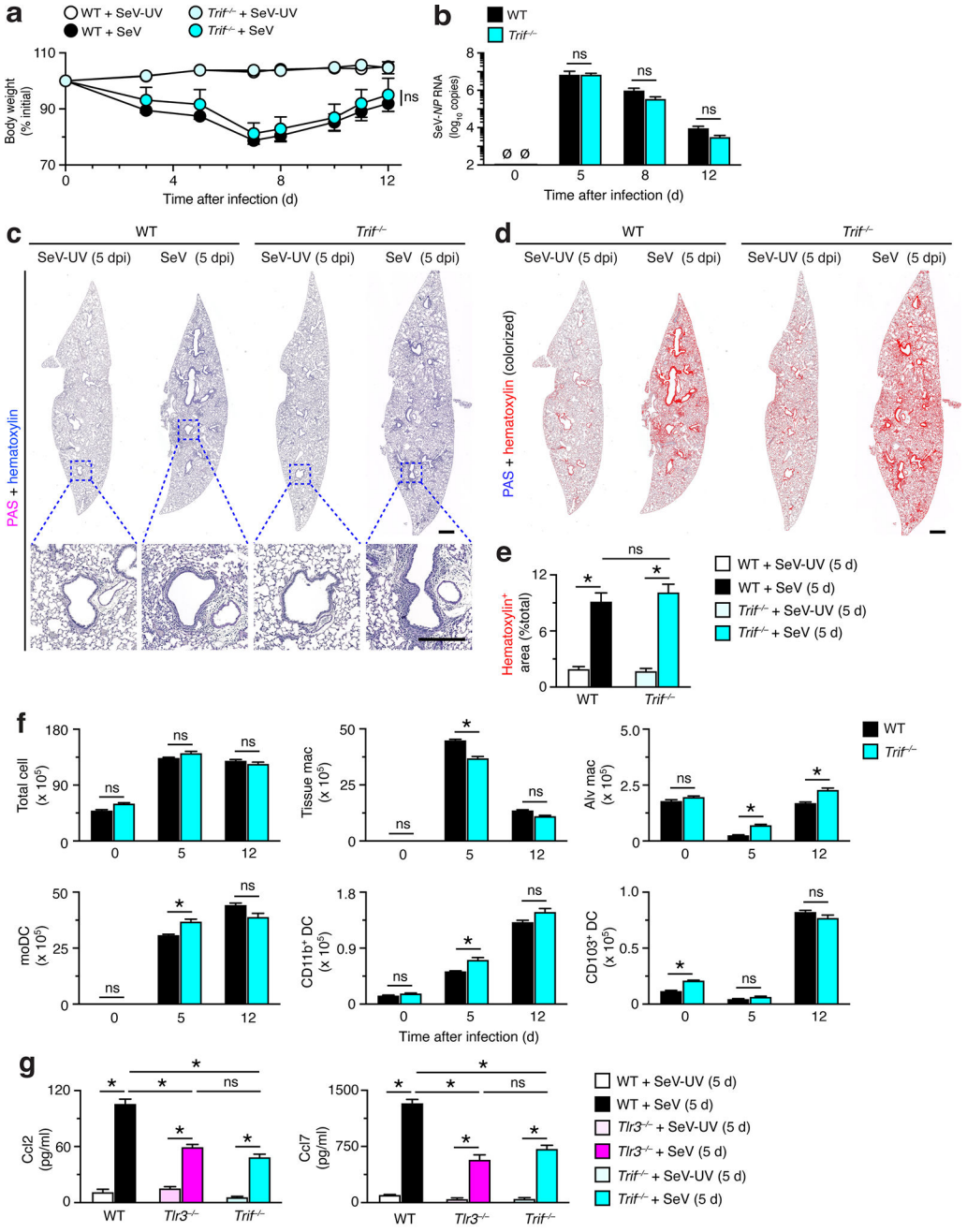

Figure 3

FIGURE 3.

TRIF-deficiency does not affect acute inflammatory illness after viral infection. (**a**) Body weights for WT and *Trif*$^{-/-}$ mice after SeV infection or SeV-UV. (**b**) Levels of SeV *NP* RNA in lungs from the same strains of mice after infection with SeV. (**c**) PAS and hematoxylin staining of lung sections from WT and *Trif*$^{-/-}$ mice at 5 d after SeV or SeV-UV. Small scale bar, 500 μm; large scale bar, 250 μm. (**d**) Lung sections from (c) with hematoxylin staining colorized red using image analysis. (**e**) Quantification of red-colorized staining from (d). (**f**) Flow cytometry-based levels of total and immune cell populations in lung tissue from WT

and *Trif*$^{-/-}$ mice at indicated time points after SeV infection. (**g**) Levels of Ccl2 and Ccl7 in lung tissue from WT, *Tlr3*$^{-/-}$, and *Trif*$^{-/-}$ mice at 5 d after SeV infection or SeV-UV. All data are representative of three separate experiments (mean and SEM) with at least 5 mice per condition in each experiment. *P<0.01.

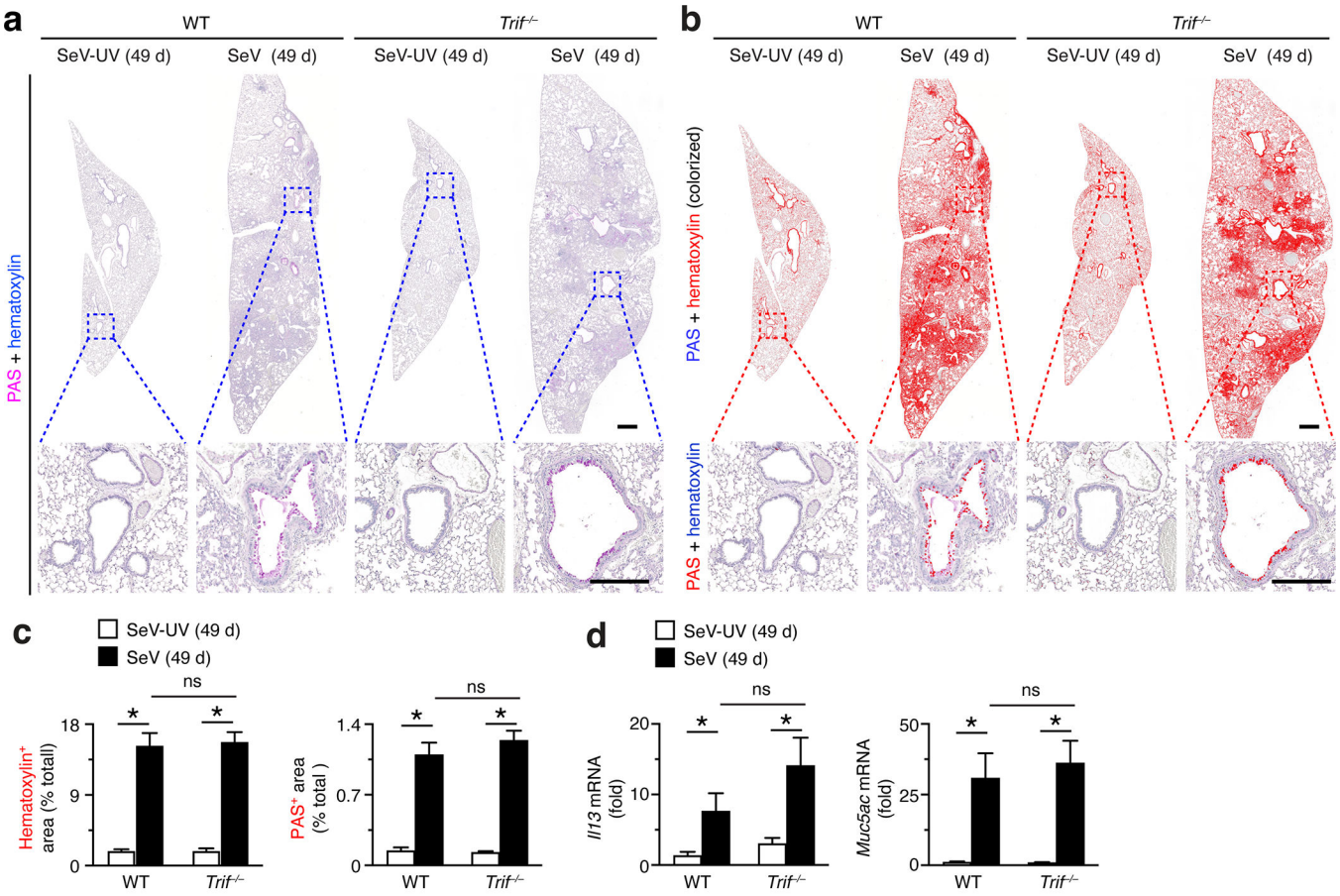

Figure 4

FIGURE 4.

TRIF-deficiency does not influence chronic lung disease after viral infection. (**a**) PAS and hematoxylin staining of lung sections from WT and *Trif*$^{-/-}$ mice at 49 d after SeV infection or SeV-UV. Small scale bar, 500 μm; large scale bar, 250 μm. (**b**) Corresponding hematoxylin and PAS staining from (a) colorized red with image analysis. (**c**) Quantification of red colorized staining from (b). (**d**) Levels of *Il13* and *Muc5ac* mRNA in lungs from WT and *Trif*$^{-/-}$ mice at 49 d after infection with SeV or SeV-UV. All data are representative of three separate experiments (mean and SEM) with at least 5 mice per condition in each experiment. *P<0.01.

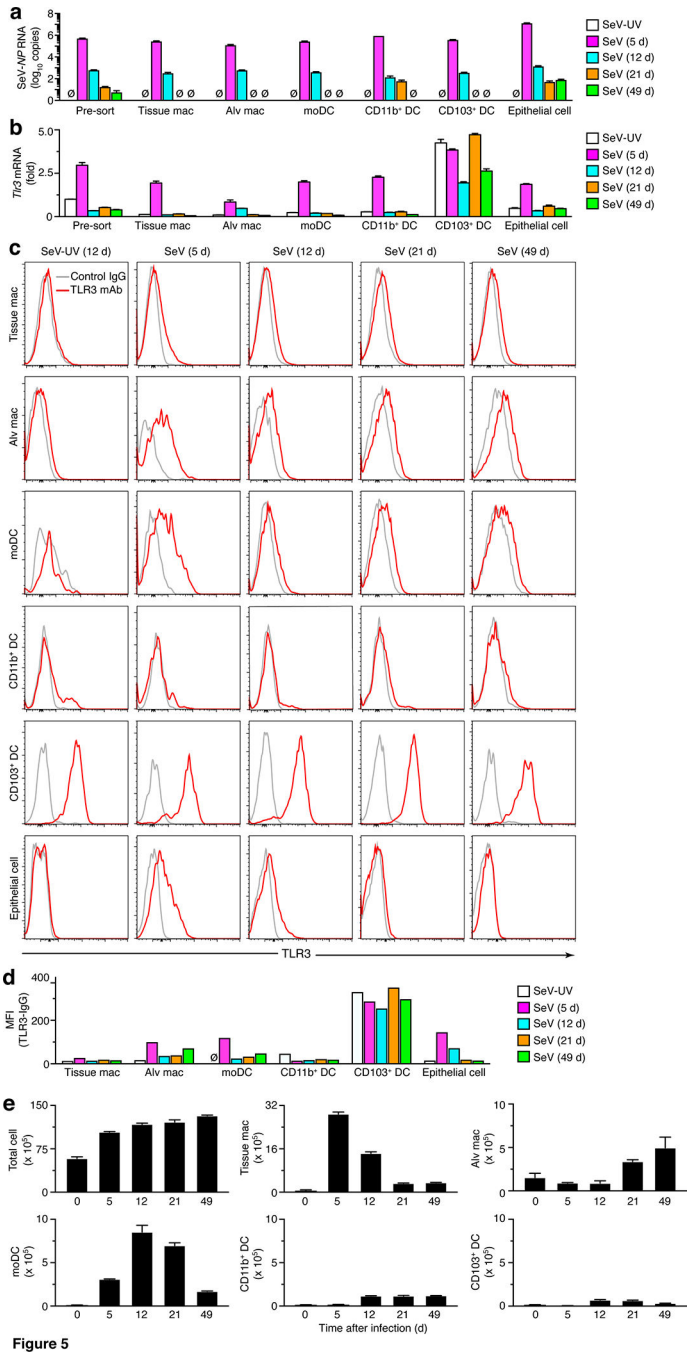

Figure 5

FIGURE 5.

Increases in viral RNA, TLR3 expression, and cell number implicate moDCs as an abundant cell site after viral infection. (**a**) Levels of SeV *NP* RNA in total cells and FACS-purified cell populations from lungs of WT mice at indicated times after SeV infection or SeV-UV. (**b**) Levels of *Tlr3* mRNA for conditions in (a). (**c**) Levels of intracellular TLR3 for conditions in (a). (**d**) Quantification of MFI for TLR3 (expressed as the value for TLR3 minus IgG control) for conditions in (a). (**e**) Levels of total and immune cell populations in lung tissue from WT mice at 5–49 d after SeV infection or control SeV-UV (0 d). All data are

representative of two to three separate experiments (mean and SEM) with at least 5 mice per condition in each experiment. *P<0.01.

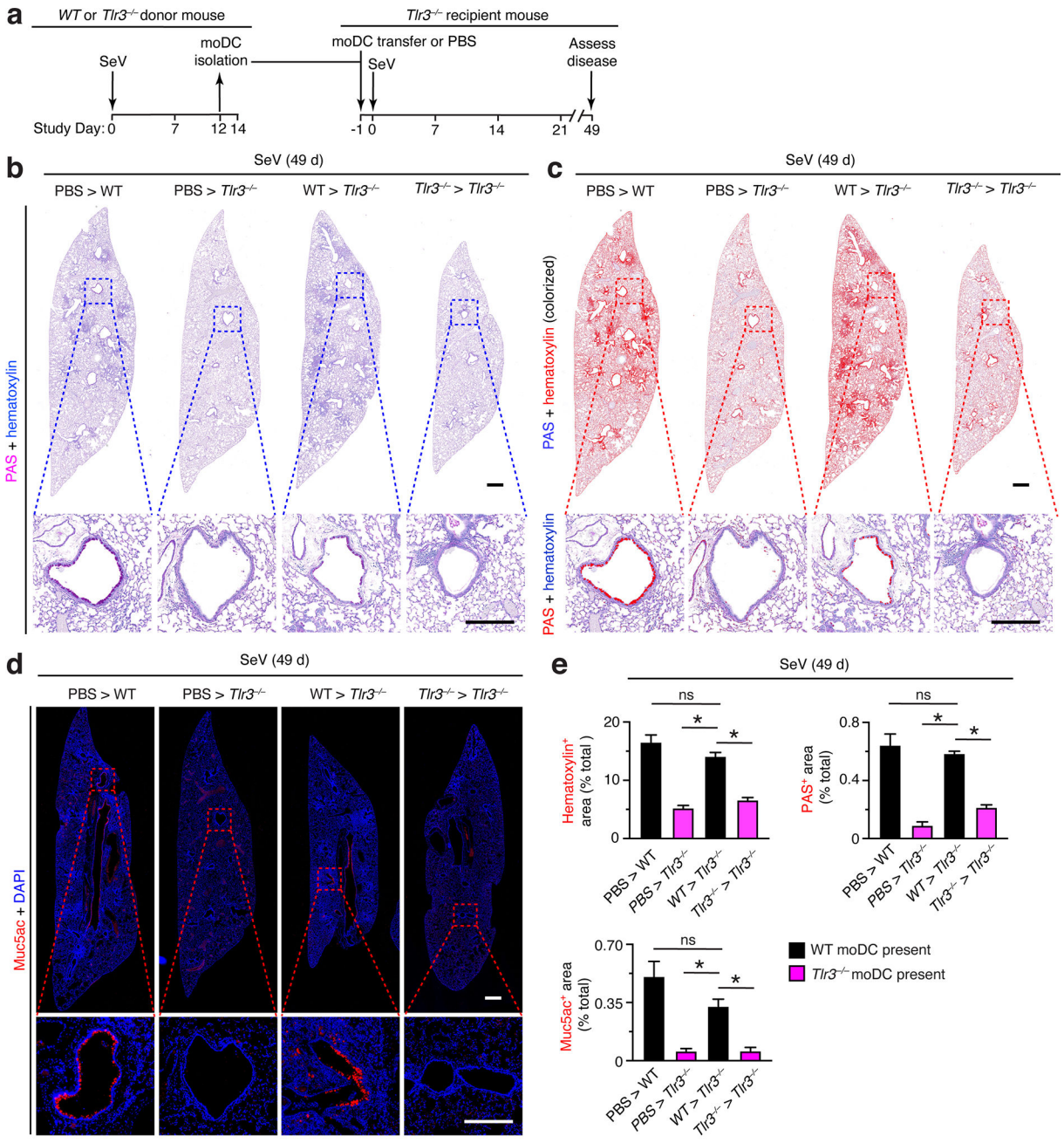

Figure 6

FIGURE 6.

Adoptive transfer of moDCs reconstitutes chronic lung disease in *Tlr3*$^{-/-}$ mice. (**a**) Protocol scheme for isolation of moDCs from lungs of WT mice, then transfer (1×10^6 cells) into *Tlr3*$^{-/-}$ mice at 1 d before SeV, and then assay for disease at 49 d after SeV infection. (**b**) PAS and hematoxylin staining of lung sections for indicated cell transfer conditions at 49 d after infection with SeV. Small scale bar, 500 μm; large scale bar, 250 μm. (**c**) Lung sections from (b) with hematoxylin and PAS staining colorized red with image analysis. (**d**) Muc5ac immunostaining of lungs for conditions in (b). Small scale bar, 500 μm; large scale bar, 250

μm. (**e**) Quantification of red colorized staining from (c) and immunostaining from (d). All data are representative of three separate experiments (mean and SEM) with at least 5 mice per condition in each experiment. *$P<0.01$.

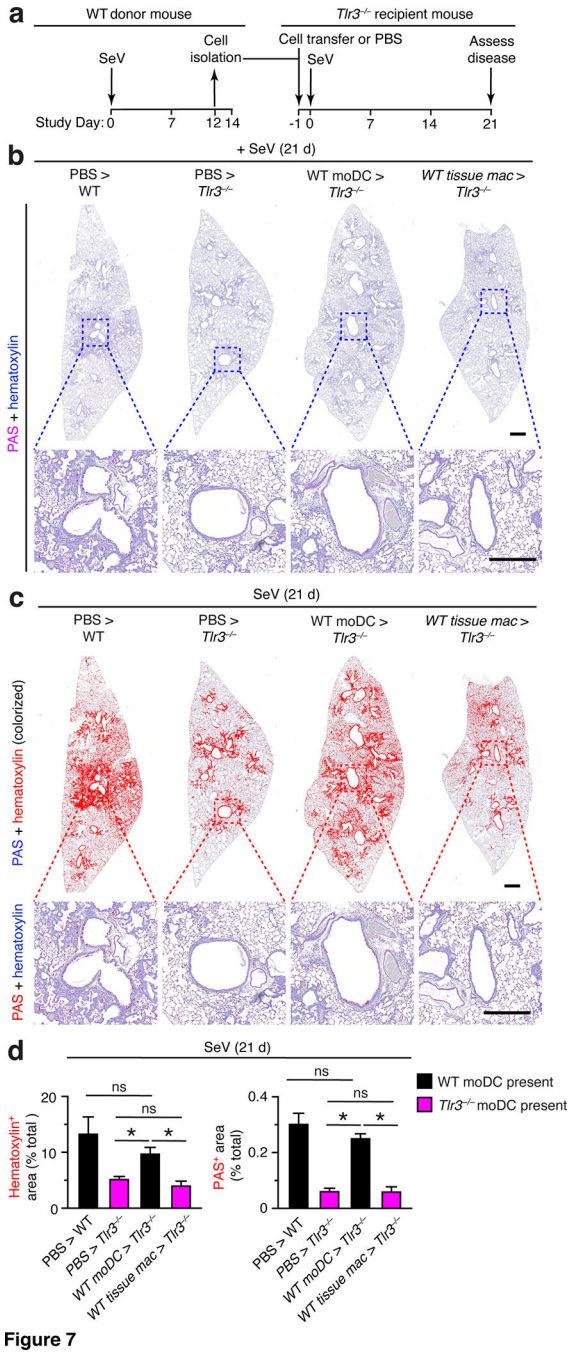

Figure 7

FIGURE 7.

Adoptive transfer of moDCs but not tissue macrophages reconstitutes chronic lung disease in *Tlr3*$^{-/-}$ mice. (**a**) Protocol scheme for isolation and transfer of moDCs or tissue macs from WT into *Tlr3*$^{-/-}$ mice. (**b**) PAS and hematoxylin staining of lung sections for indicated cell transfer conditions at 21 d after SeV infection. Small scale bar, 500 μm; large scale bar, 250 μm. (**c**) Lung sections from (b) with hematoxylin and PAS staining colorized red with image analysis. (**d**) Quantification of red colorized staining from (c). All data are representative of

three separate experiments (mean and SEM) with at least 5 mice per condition in each experiment. *P<0.01.

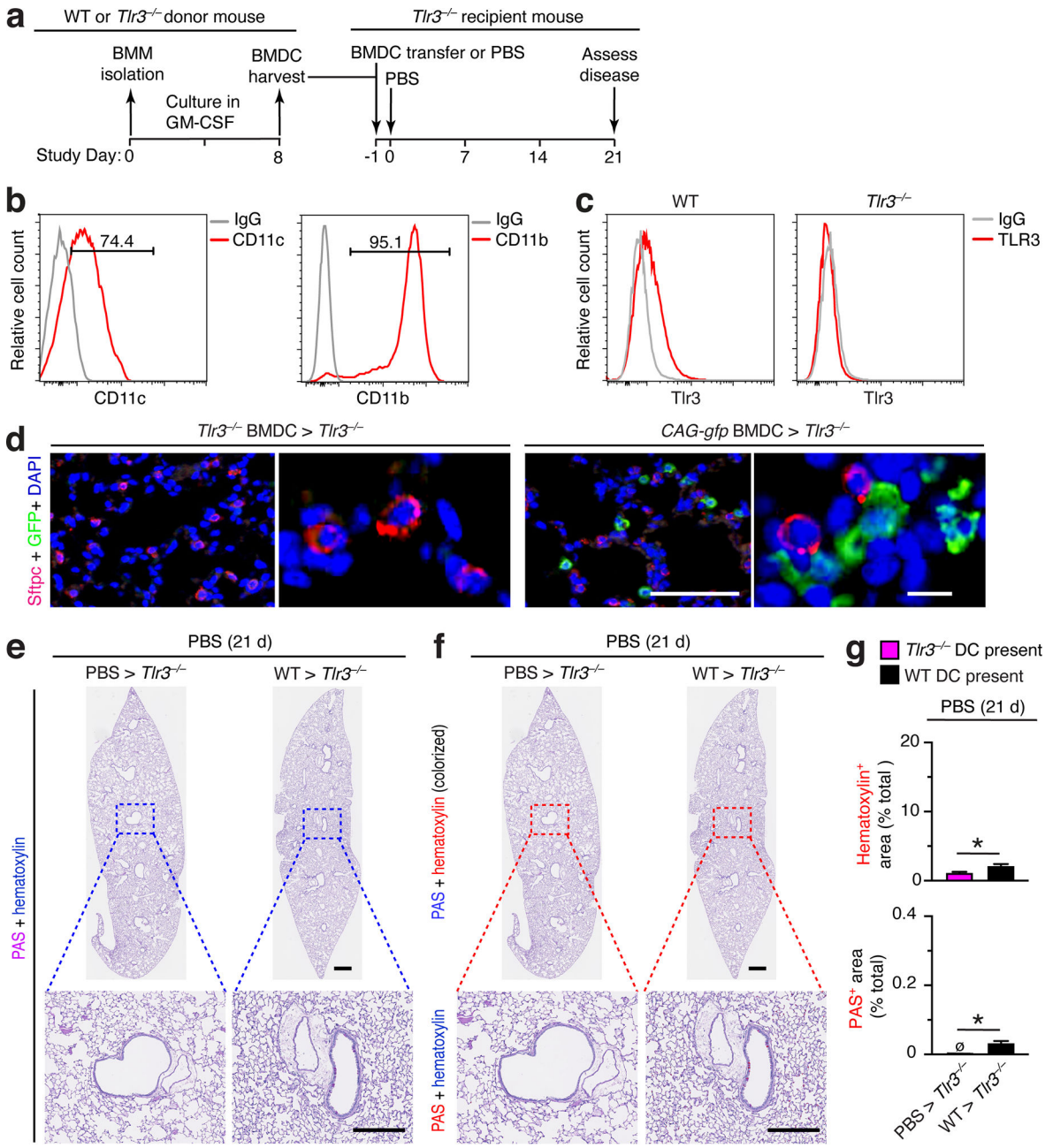

Figure 8

FIGURE 8.

Adoptive transfer of BMDCs causes minor lung disease without viral infection in *Tlr3*$^{-/-}$ mice. (**a**) Protocol scheme for isolation and transfer of BMDCs from WT into *Tlr3*$^{-/-}$ mice. (**b**) Histograms from flow cytometry analysis of CD11c^{+} and CD11b^{+} cells in BMDC cultures for conditions in (a). (**c**) Histograms for intracellular TLR3 in BMDCs from WT or *Tlr3*$^{-/-}$ mice for conditions in (b). (**d**) Immunostaining for Sftpc and GFP and counterstaining for DAPI of lung sections from *Tlr3*$^{-/-}$ mice at 1 d after transfer of BMDCs from *Tlr3*$^{-/-}$ or *CAG-gfp* mice (0 d after SeV infection). Large scale bar, 100 μm; small

scale bar, 10 μm. (**e**) PAS and hematoxylin staining of lung sections for indicated cell transfer conditions at 21 d after PBS. Small scale bar, 500 μm; large scale bar, 250 μm. (**f**) Lung sections from (e) with hematoxylin and PAS staining colorized red with image analysis. (**g**) Quantification of colorized staining from (f). All data are representative of three separate experiments (mean and SEM) with at least 5 mice per condition in each experiment. *$P<0.01$.

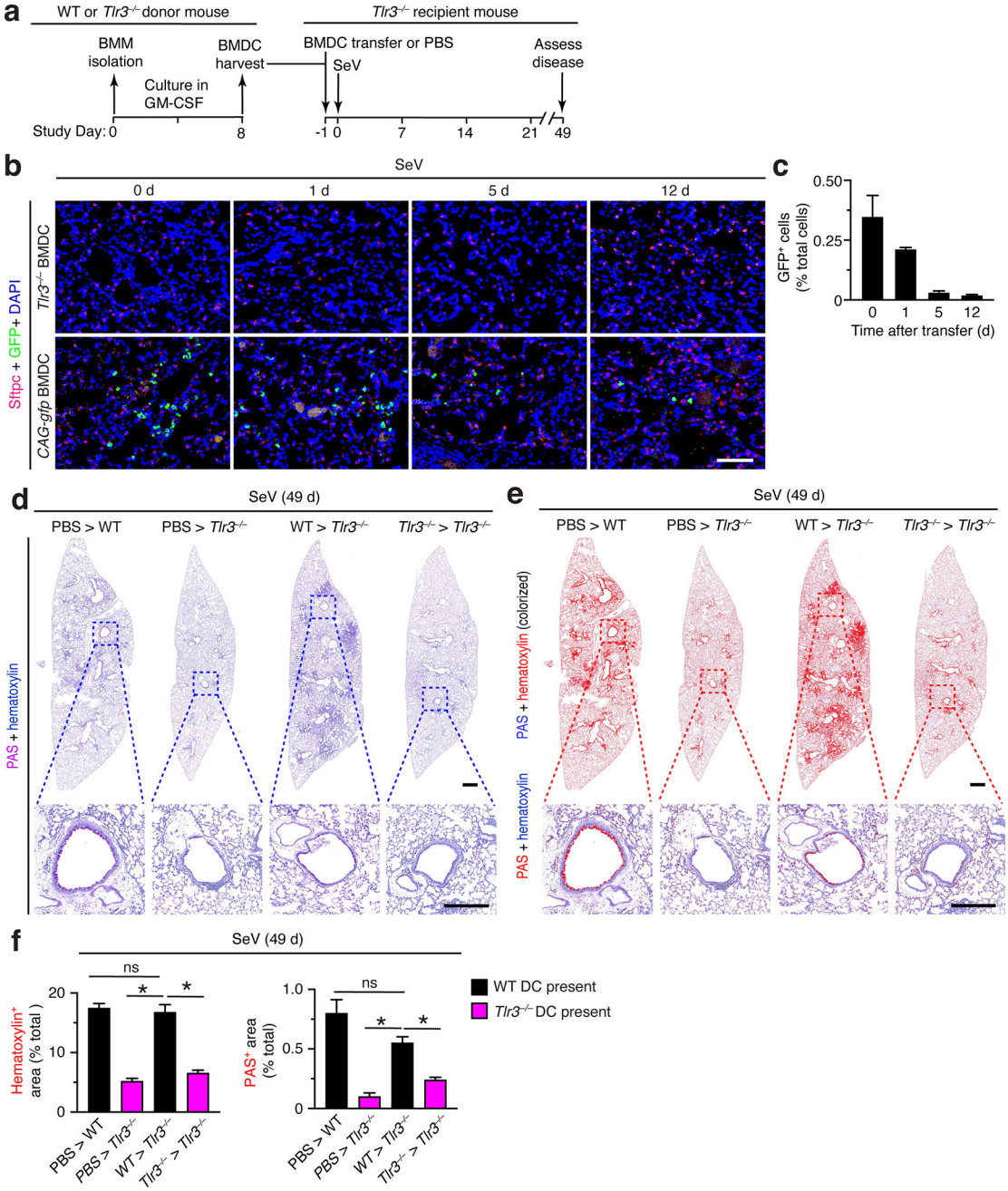

Figure 9

FIGURE 9.

Adoptive transfer of BMDCs reconstitutes chronic lung disease after viral infection in *Tlr3*$^{-/-}$ mice. (**a**) Protocol scheme for isolation and transfer of BMDCs from WT into *Tlr3*$^{-/-}$ mice. (**b**) Immunostaining for Sftpc and GFP and counterstaining for DAPI of lung sections from *Tlr3*$^{-/-}$ mice after transfer of BMDCs from *Tlr3*$^{-/-}$ or *CAG-gfp* mice and then 0–12 d after SeV infection. Scale bar, 100 μm. (**c**) Quantification of GFP^{+} immunostaining from (b). (**d**) PAS and hematoxylin staining of lung sections for indicated cell transfer conditions at 49 d after infection with SeV. Small scale bar, 500 μm; large scale bar, 250 μm. (**e**) Lung

sections from (c) with hematoxylin and PAS staining colorized red with image analysis. (**f**) Quantification of colorized staining from (d). All data are representative of three separate experiments (mean and SEM) with at least 5 mice per condition in each experiment. **P*<0.01.

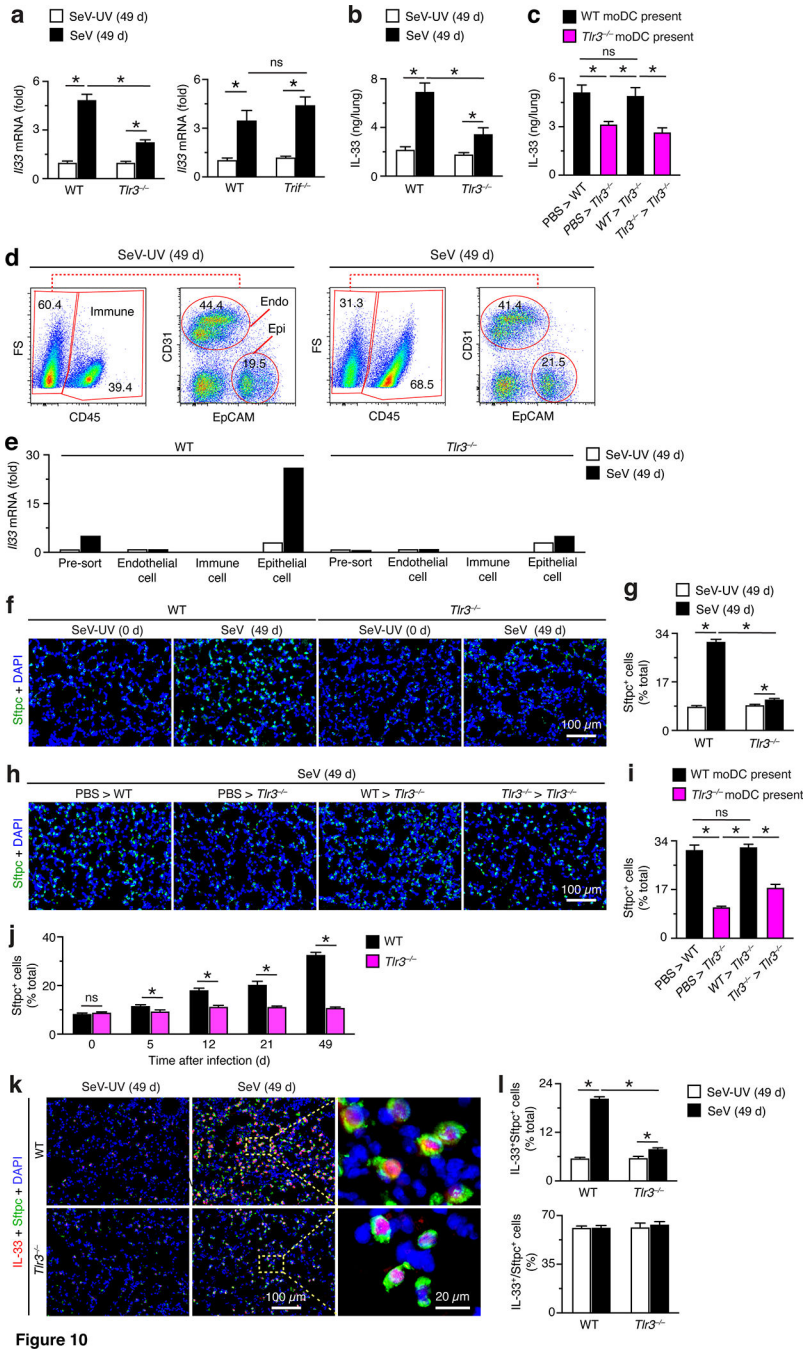

Figure 10

FIGURE 10.

TLR3-moDC-driven disease depends on expansion of IL-33-expressiong AT2 cells. (**a**) Levels of *Il33* mRNA in lungs from WT, *Tlr3*$^{-/-}$, and *Trif*$^{-/-}$ mice at 49 d after SeV infection or SeV-UV. (**b**) Levels of IL-33 per lung from WT and *Tlr3*$^{-/-}$ mice at 49 d after SeV or SeV-UV. (**c**) Levels of IL-33 in lungs from indicated cell transfer conditions. (**d**) Flow cytometry analysis of CD31^{+} endothelial cells, CD45^{+} immune cells, EpCAM^{+} epithelial cells at 49 d after SeV or SeV-UV. (**e**) Levels of *Il33* mRNA in cell populations from (d) in WT and *Tlr3*$^{-/-}$mice at 49 d after SeV or SeV-UV. (**f**) Immunostaining for Sftpc with DAPI

counterstaining in lung sections from WT and *Tlr3*$^{-/-}$ mice at 49 d after SeV or SeV-UV. Scale bar, 100 μm. (**g**) Quantification of staining from (f). (**h**) Immunostaining for Sftpc with DAPI counterstaining in lung sections from indicated cell transfer conditions at 49 d after SeV. Scale bar, 100 μm. (**i**) Quantification of staining from (h). (**j**) Levels of Sftpc-expressing cells in lungs of WT and *Tlr3*$^{-/-}$ mice at indicated times after SeV infection. (**k**) Immunostaining for IL-33 and Sftpc for conditions in (f). Scale bars, 100 and 20 μm as indicated. (**l**) Quantitation of staining from (k) for IL-33^{+}Sftpc^{+} cells as percent of total cells (% total) and for IL33^{+} cells as percent of Sftpc^{+} cells (%). All data are representative of three separate experiments (mean and SEM) with at least 5 mice per condition in each experiment. *P<0.01.

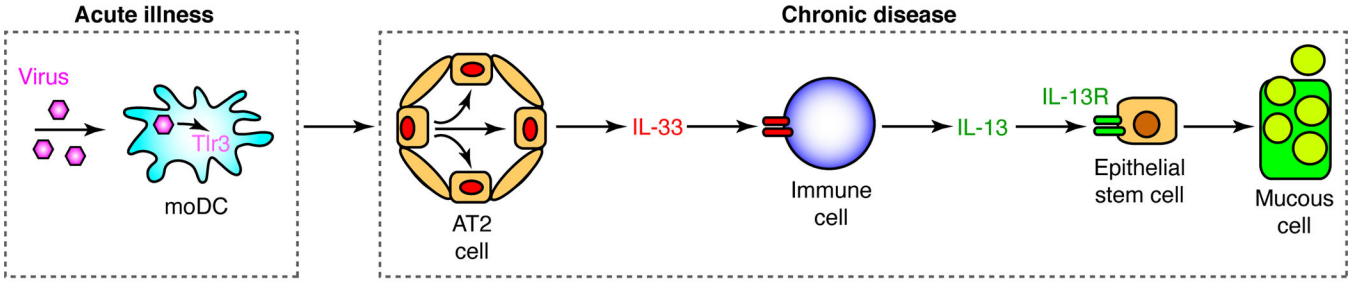

Figure 11

FIGURE 11.

Scheme for TLR3-activated moDCs in chronic lung disease. Initial viral replication in DCs activates TLR3 signaling that drives expansion of AT2 cells as a predominant cell source of IL-33 that acts on downstream immune cells (ILC2s and tissue macrophages) to drive IL-13 production and consequent epithelial stem cell differentiation to mucous cells for mucus production that is characteristic of chronic lung disease.